PROTEINS: Structure, Function, and Bioinformatics 56:67–84 (2004)

Toward the Active Conformations of Rhodopsin and the β_2-Adrenergic Receptor

Paul R. Gouldson,[1] Nathan J. Kidley,[2] Robert P. Bywater,[3] Georgios Psaroudakis,[2] Harry D. Brooks,[2] Constantino Diaz,[4] David Shire,[4] and Christopher A. Reynolds[2]*

[1]*Deffinity Solutions Ltd., Hampshire, United Kingdom*
[2]*Department of Biological Sciences, University of Essex, Colchester, Essex, United Kingdom*
[3]*Novo Nordisk A/S, Måløv, Denmark*
[4]*Sanofi-Synthelabo Recherche, Centre de Labège, Labège, France*

ABSTRACT **Using sets of experimental distance restraints, which characterize active or inactive receptor conformations, and the X-ray crystal structure of the inactive form of bovine rhodopsin as a starting point, we have constructed models of both the active and inactive forms of rhodopsin and the β_2-adrenergic G-protein coupled receptors (GPCRs). The distance restraints were obtained from published data for site-directed crosslinking, engineered zinc binding, site-directed spin-labeling, IR spectroscopy, and cysteine accessibility studies conducted on class A GPCRs. Molecular dynamics simulations in the presence of either "active" or "inactive" restraints were used to generate two distinguishable receptor models. The process for generating the inactive and active models was validated by the hit rates, yields, and enrichment factors determined for the selection of antagonists in the inactive model and for the selection of agonists in the active model from a set of nonadrenergic GPCR drug-like ligands in a virtual screen using ligand docking software. The simulation results provide new insights into the relationships observed between selected biochemical data, the crystal structure of rhodopsin, and the structural rearrangements that occur during activation. Proteins 2004;56:67–84.** © 2004 Wiley-Liss, Inc.

Key words: G-protein coupled receptor; rhodopsin; adrenergic; molecular modeling; active conformation; inactive conformation; docking; agonist; antagonist

INTRODUCTION

Members of the integral membrane G-protein coupled receptor (GPCR) family mediate many vital cellular signaling processes in eukarya. The landmark determination of the X-ray structure of a GPCR, rhodopsin,[1] has given rise to new opportunities (e.g., for constructing models of other GPCRs by homology modeling). However, the only crystal structure to date is that of an inactive (dark state) form of the receptor. Consequently, we have systematically separated a wealth of additional structural data into data relevant to the inactive form and that relevant to the active form, with a view toward employing this data to study the active form of the receptor. The underlying assumption in this work is that the active forms of the receptor share common structural features, and this can be justified by both chimeric receptor studies (see Zhao et al.[2] and similar site-directed mutagenesis effects at corresponding residues (see below); the assumption that the inactive forms of the receptor share common structural features can also be justified by evaluating structural data derived from receptors other than rhodopsin against the rhodopsin structure (see Table I).

The structural data include site-directed spin labeling (SDSL) experiments that involve crosslinking of cysteine residues with nitroxides, followed by electron paramagnetic resonance (EPR) spectroscopy to determine interatomic distances; this technique has given extensive data on the structural changes that occur during rhodopsin photoactivation, most notably the movement of transmembrane helices upon activation.[3–12] The introduction of zinc-binding sites was used to demonstrate unequivocally that the transmembrane helices of the NK1 tachykinin receptor were orientated in an anticlockwise fashion[13]; engineered zinc-binding sites have also been used to study both inactive and active receptor conformations.[14–19] The substituted cysteine accessibility method (SCAM) has proved a powerful technique for determining the transmembrane (TM) residues that form the interior polar cavity of the dopamine D_2 receptor[20–23]; SCAM has also been used to monitor conformational changes that occur in transmembrane helix 6 (TM6) of a constitutively active β_2-adrenergic (β_2-AR) receptor.[24] SDCL studies have provided the most illuminating structural details for the active receptor conformation; analysis of disulfide bond formation for native and introduced cysteine residues has demonstrated that large structural changes may occur during receptor activation.[25–28] An alternative crosslinking method that has been used for rhodopsin involves incorporating photo-

Grant sponsor: Novo Nordisk A/S (to P. R. Gouldson). Grant sponsor: Engineering and Physical Sciences Research Council (EPSRC) (to N. J. Kidley). Grant sponsor: Royal Society/Wolfson Foundation.

*Correspondence to: Christopher A. Reynolds, Department of Biological Sciences, University of Essex, Colchester, Essex, CO4 3SQ, UK. E-mail: c.a.reynolds@essex.ac.uk

Received 14 August 2003; Accepted 2 December 2003

Published online 16 April 2004 in Wiley InterScience (www.interscience.wiley.com). DOI: 10.1002/prot.20108

TABLE I. Relative Residue and Atomic Restraints Associated With Inactive GPCRs

Experimental evidence	Rhodopsin X-ray structure distances	Restraint in receptor model
Disulfide formation between Cys^{140}(gn345) & Cys^{222}(gn527) in dark state rhodopsin.[26a]	r(S-S) = 7.6	Normal r(S-S) restraint or equivalent r(Cγ-Cγ) restraint between Thr^{136}(gn345) & Val^{218}(gn527), but following used instead.[a]
Disulfide formation between H65C(gn140) & Cys^{316}(gn743) in dark state rhodopsin.[11]	r(S-S) = 7.1 Å	Normal r(S-S) restraint or equivalent r(Cγ-Cγ) restraint between Phe^{61}(gn140) & Phe^{336}(gn743).
Crosslink of retinal β-ionone ring position C-3 to Trp^{265} in dark state of rhodopsin.[29]	r(C-X) ≈ 3.8 Å	Not applicable[c]
Zinc-binding site inactivates β_2-AR A134H(gn343) & E268H(gn600).[16]	r(Cα-Cα) = 6.5 Å/r(N-N) = 6.4 Å	r(Cα-Cα) < 10 Å, N-N < 6 Å; restraint between A134H(gn343) & E268H(gn600).
Zinc-binding site inactivates β_2-AR A134H(gn343) & His^{269}(gn601).[16]	r(Cα-Cα) = 8.4 Å/r(N-N) = 5.9 Å	r(Cα-Cα) < 10 Å, N-N < 6 Å; restraint between A134H(gn343) & His^{269}(gn601).[16]
Engineered zinc binding site inactivates β_2-AR A134H(gn343)-L272H(gn604).[16]	r(Cα-Cα) = 11.3Å/r(N-N) = 7.2Å	r(Cα-Cα) < 10 Å, N-N < 6 Å; restraint between A134H(gn343)- L272H(gn604).[d]
Average distance between V139C(gn344)-K248C(gn601) & V139C(gn344)-T251C(gn604); mutants reacted with nitroxide in dark state.[8]	r[O(139)-O(248)] = 14.3 Å r[O(139)-O(251)] = 14.5 Å	r(O-O) ≈ 12–14 Å; restraint between nitroxide reacted with Ile^{135}(gn344)-His^{269}(gn601)[d] & Ile^{135}(gn344)-Leu^{272}(gn604).[c,d]
Average distance between V139C(gn344)-E249C(gn602), V139C(gn344)-V250C(gn603), & V139C(gn344)-R252C(gn605); mutants reacted with nitroxide in dark state.[8]	r[O(139)-O(249)] = 21.3 Å r[O(139)-O(250)] = 19.3 Å r[O(139)-O(242)] = 19.7 Å	r(O-O) ≈ 15–20 Å; restraint between nitroxide reacted with Ile^{135}(gn344)-Lys^{249}(gn602),[d] Ile^{135}(gn344)-Ala^{250}(gn603)[d] & Ile^{135}(gn344)-Lys^{252}(gn605).[c,d]
Engineered zinc-binding site in M_1 receptor between L116H(gn333)-S120H(gn337)-F374H(gn614).[15]	r(Cα-Cα) = 6.3 Å/r(N-N) = 2.6 Å r(Cα-Cα) = 10.1 Å/r(N-N) = 4.2 Å r(Cα-Cα) = 13.5 Å/r(N-N) = 7.4 Å	r(Cα-Cα) < 10 Å, r(N-N) < 6 Å; restraint between Leu^{124}(gn333), Ala^{128}(gn337), & Phe^{282}(gn614).[e,f]
Engineered zinc-binding site in M_1 receptor between L116H(gn333)-F374H(gn614)-N414(gn729).[15]	r(Cα-Cα) = 11.5 Å/r(N-N) = 4.1 Å r(Cα-Cα) = 7 Å/r(N-N) = 1.3 Å r(Cα-Cα) = 10 Å/r(N-N) = 4.8 Å	r(Cα-Cα) < 10 Å, N-N < 6 Å; restraint between Leu^{124}(gn333), Phe^{282}(gn614), & Asn^{322}(gn729); gn333-gn614 only used in rhodpsin; gn333–gn729 not applicable—due to bridging water?
Engineered zinc-binding site in M_1 receptor between F374H(gn614)-N414H(gn729)-Y418(gn733).[15]	r(Cα-Cα) = 7 Å/r(N-N) = 1.3 Å r(Cα-Cα) = 6.2 Å/r(N-N) = 2.2 Å r(Cα-Cα) = 11.3 Å/r(N-N) = 1.5 Å	r(Cα-Cα) < 10Å, N-N < 6 Å; Restraint between Phe^{282} gn614, Asn^{322}(gn729), & Tyr^{326}(gn733).[e]
Natural zinc-binding site in NK1 receptor between His^{197}(gn509)-His^{265}(gn622)[156]	r(Cα-Cα) = 9.6 Å/r(N-N) = 4.7 Å	r(Cα-Cα) < 10Å, N-N < 6 Å; restraint between Ala^{200}(gn509)-Phe^{290}(gn622).
Increased zinc-binding affinity with engineered binding site in NK1 receptor between E193H(gn505)-Y272H(gn629).[156]	r(Cα-Cα) = 9.6 Å/r(N-N) = 5.2 Å	r(Cα-Cα) < 10 Å, N-N < 6 Å; restraint between Asn^{196}(gn505) & Val^{297}(gn629).
Increased zinc-binding affinity with engineered zinc-binding site in NK1 receptor with mutant T201H(gn513).[156]	r(Cα-Cα) = 9.7 Å/r(N-N) = 4.7 Å r(Cα-Cα) = 6.1 Å/(N-N) = 3.6 Å r(Cα-Cα) = 7.8 Å/N-N = 1.1 = Å	r(Cα-Cα) < 10 Å, N-N < 6 Å; restraint between Ala^{200}(gn509)-Phe^{290}(gn622) & Ser^{204}(gn513).[e]
Increased zinc-binding affinity with engineered zinc-binding site in NK1 receptor with mutant L269H(gn626).[156]	r(Cα-Cα) = 9.7 Å/r(N-N) = 4.7 Å r(Cα-Cα) = 5.9 Å/r(N-N) = 2.2 Å r(Cα-Cα) = 7.3 Å/r(N-N) = 4.8 Å	r(Cα-Cα) < 10 Å, N-N < 6 Å; restraint between Ala^{200}(gn509)-Phe^{290}(gn622) & Ile^{294}(gn626).[e]
Interaction of Glu^{122}(gn318) & His^{211}(gn516) in rhodopsin.[157]	r(Cα-Cα) = 10.3 Å	r(Cα-Cα) < 8 Å; restraint between Thr^{118}gn(327) & Ser^{207}(gn516).[c]
Cys^{285} inaccessible to aqueous probes.[24b]	No applicable distance restraint	Cys^{285}(gn617) at helix–helix or helix–lipid interface.

[a]Rate of disulfide reaction very slow in the dark state bovine rhodopsin, implying a large separation.
[b]The restraint associated with the SCAM data studies on constitutively active mutant β_2-AR cannot be included explicitly as a restraint, but served as a check on the final structure.
[c]Distance restraints used as a check on the final structure.
[d]Only used in β_2-AR because of ligand position.
[e]Restraints not used within the same helix.
[f]Only used in rhodopsin.

TABLE II. The X-ray, Sequence, and Generic Numbers (GPCRDB and Ballesteros) for the Maximum Extent of Helix Ends, as Determined by the Database of Secondary Structures in Proteins

TM	Rhodopsin X-ray	β_2-AR X-ray	Generic	
			GPCRDB	Ballesteros
1	34–64	30–60	109–139	1.28–1.58
2	71–100	67–96	212–241	2.38–2.67
3	106–140	102–136	311–345	3.21–3.55
4	150–175	147–172	409–434	4.39–4.64
5	199–230	195–226	504–535	5.34–5.65
6	246–277	267–298	599–630	6.29–6.60
7	285–309	305–329	712–736	7.32–7.56

Where the helix ends differ among the 4 different models, the numbers giving the longest helix are recorded.

active groups into ligand structures to provide details on ligand–receptor interactions.[29–32]

However, care must be taken when using this additional structural data, particularly with regard to whether the data correspond to active or inactive conformations. Thus, for site-directed mutagenesis data, the effects of mutations on inverse agonists/antagonists and agonists must be treated separately. To date, many models have incorporated site-directed mutagenesis data for *all* classes of ligands to generate one receptor model. This results in an averaging of the models to a state that represents neither an active nor an inactive receptor, even if simulations are then performed in the presence of agonists or antagonists. Relatively few models have been built with at least two receptor conformations in mind,[33,34] but the lack of a recognized systematic approach to generating both active and inactive conformations is one plausible origin for the discrepancies that occur between models, and between models and experiment.[35–39]

In order to address this problem, restrained molecular dynamics (MD) has been used to generate active (and inactive) conformational models of the human β_2-AR receptor and rhodopsin, with a view toward using these models in further biochemical experiments on the molecular mechanisms that govern ligand interactions and receptor activation.

COMPUTATIONAL METHODS

Construction of the Initial Receptor Models

The model of the β_2-AR receptor was built from the 2.8 Å rhodopsin structure[40] [Protein Data Bank (PDB) code: 1F88] using the correspondences defined in the profile-based multiple sequence alignment of the β_2-AR and rhodopsin receptor families. Here and elsewhere the residues are identified by the sequence number in bovine rhodopsin or the rat β_2-AR receptor, and by their GPCR Database (GPCRDB)[41] global number (gn)[42] (see Table II). The undefined region of IL3 (Gln^{236}-Glu^{239}) in rhodopsin was added by searching for the best insert available in a refined protein structural database based on criteria such as gap closure distance and backbone atom position; sequence conservation was taken into account through user inspection of potential loop conformations. The large IL3 (Lys^{232}-Leu^{258}) and C-terminus (Ser^{347}-Leu^{383}) of the β_2-AR receptor were not included in the receptor model. A protein–ligand interaction modeler (PLIM)[43] was used to add 580 explicit water molecules to solvate the extracellular loops, intracellular loops, and the TM helical bundle cavity through an iterative process whereby water molecules were added in batches of 10, followed by energy minimization employing a 15 Å nonbonded cutoff for the electrostatics and van der Waals terms, and a 30° step angle for finding the best hydrogen-bond geometries.

Several approaches for modeling the membrane environment are possible. One approach is to carry out full lipid simulations on fully hydrated bilayers (or bilayer mimics) as the hydrophobic lipid chains provide packing forces and the solvent region provides dielectric screening. However, these methods are generally used for structural studies on channels that undergo limited conformational changes (e.g., see references[44–48]). Few membrane simulation studies have seriously addressed the true composition of the lipid but rather deal with ideal systems. Moreover, for systems undergoing large conformational changes, it is more usual to omit the solvent and the lipid (as the lipid can hinder motion, reduce conformational sampling, and trap the structure in abortive local minima), and introduce dielectric screening via a distance-dependent dielectric.

Indeed, in a rare study of GPCR activation in a fully hydrated bilayer, Rohrig et al.[49] admit that the simulations do not sufficiently model the receptor movement. In contrast, the stochastic boundary MD study of aquaporin[50] included more discussion of protein structural changes than related hydrated bilayer studies.[46] Consequently, the use of simplified methods is the usual approach for implementing NMR restraints[51,52] and by analogy is a natural choice for the simulations described here. Studies on the effect of mutations on redox potentials have shown that a distance-dependent dielectric constant can give reliable predictions,[53] and while the reported optimum screening was provided by an exponential function, here we have opted for a 1/r function, since some screening is implemented explicitly through the incorporation of the explicit water molecules. Moreover, McCammon and coworkers have shown that a few layers of explicit water molecules are an important adduct to a continuum treatment of a membrane environment,[54] and while McCammon's Poisson–Boltzmann continuum treatment is more sophisticated than that used here, the combination of continuum plus explicit water is nevertheless well founded.

The 11-cis and all trans conformations of retinal were docked into the crystal structure using interactive molecular graphics, thus generating two initial rhodopsin models.

The solvated receptor models were subjected to MD simulations involving a 100 ps heating stage from 0 K to 310 K, a further 200 ps at 310 K, and then a conjugate gradient minimization to yield the initial solvated receptor models.

TABLE III. Relative Residue and Atomic Restraints Associated With Active GPCRs

Experimental evidence	Rhodopsin X-ray distances	Restraint in receptor model
Disulfide formation between Cys^{140}(gn345) and Cys^{316}(gn743) in rhodopsin upon photo bleaching.[26]	r(S-S) = 25.5 Å	Normal r(S-S) restraint or equivalent r(Cγ-Cγ) restraint between Thr^{136}(gn345) & Phe^{332}(gn743).
Increased rate of disulfide reaction between Cys^{140}(gn345) & Cys^{222}(gn527) in rhodopsin on photo bleaching.[85]	r(S-S) = 7.1 Å	Normal r(S-S) restraint or equivalent r(Cγ-Cγ) restraint between Thr^{136}(gn345) & Val^{218}(gn527).
Crosslink of retinal β-ionone ring position C-3 to Ala^{169} in active state of rhodopsin.[29]	r(C-C) = 15.1 Å	3.0 Å < r(C-Cβ) < 4.0 Å; not applicable to β_2-AR.
Zinc-binding to D113C(gn322)/N312H(gn719) mutant β_2-AR causes some receptor activity.[17]	r(S-N) = 11 Å	r(Cα-Cα) < 10 Å, r(N-N) < 6 Å; restraint between Asp^{113}(gn322) & Asn^{312}(gn719).
Increased average distance between V139C(gn344)-K248C(gn601), V139C(gn344)-T251C(gn604), and V139C(gn344)-R252C(gn605); rhodopsin mutants reacted with nitroxide upon photo bleaching.[8]	r(Cα-Cα) = 6.7 Å, 10.0 Å, & 14.0 Å, respectively. r(Cβ-Cβ) = 6.0 Å, 9.5 Å, & 14.5 Å, respectively.	Initial r(O-O) ≈ 23 Å restraint between nitroxide reacted with 1135C (gn344)-H269C?(gn601), 1135C (gn344) L272C?(gn604), & 1135C (gn344)-K273C?(gn605). Subsequent rhodopsin restraints/Å, respectively: 16.0 > r(Cα-Cα) < 17.0; 17.0 < r(Cβ-Cβ) < 18.0; 16.0 > r(Cα-Cα) < 17.0; 16.5 < r(Cβ-Cβ) < 17.5; 19.6 > r(Cα-Cα) < 20.6; 21.0 < r(Cβ-Cβ) < 22.0. Subsequent β_2-AR restraints/Å, respectively: 16.2 > r(Cα-Cα) < 8; 15.8 > r(Cα-Cα) < 16.4; 16.5 < r(Cβ-Cβ) < 17.1.
No change in distance between V139C(gn344)-E249C(gn602) rhodopsin mutant reacted with nitroxide upon photo bleaching.[8]	r(Cα-Cα) = 10.4 Å r(Cβ-Cβ) = 10.6 Å	Initially, r(O-O) ≈ 15–20 Å; restraint between nitroxide reacted with 1135C (gn344)-K270C?(gn602). Subsequent rhodopsin restraints/Å, respectively: 13.3 > r(Cα-Cα) < 15.3; 11.4 < r(Cβ-Cβ) < 13.4.
Decrease in V139C(gn344)-V250C(gn603) distance; rhodopsin mutant reacted with nitroxide upon photo bleaching.[8]	r(Cα-Cα) = 10.4 r(Cβ-Cβ) = 10.2	Initially, r(O-O) ≈ 12–14 Å; restraint between nitroxide reacted with 1135C(gn344)-A271C?(gn603); Subsequent rhodopsin restraints/Å respectively: 15.0 > r(Cα-Cα) < 17.0; 15.3 < r(Cβ-Cβ) < 17.3.
Expected distance between Asp^{113}(gn322) and Ser^{204}(gn513) derived from ligand structures.[158]	r(Cγ-Cγ) = 17.0 Å	8 Å < r(Cγ-Cγ) < 10 Å restraint between Asp^{113}(gn322) & Ser^{204}(gn513).
Expected distance between Asp^{113}(gn322) and Ser^{207}(gn516) derived from ligand structures.[158]	r(Cγ-Cγ) = 15.7 Å	8 Å < r(Cγ-Cγ) < 10 Å restraint between Asp^{113}(gn322) & Ser^{207}(gn516).
Cys^{285} accessible to aqueous probes upon CAM.[24]	No applicable distance restraint.	Cys^{285}(gn617) accessible to polar pocket.

Restraints for Inactive and Active Receptor Conformations

Restraints for residues and atoms relevant to inactive and active receptor conformations were calculated primarily from SDSL and SCAM, and engineered zinc-binding data and are given in Tables I and III, respectively; the tables also show the actual distances observed in the rhodopsin crystal structure. The restraints from the SDCL are particularly important, since the structure of a disulfide bond is well defined and is chemically compatible with protein structures in general. Moreover, zinc is coordinated by His in a well-defined manner,[55] but distance restraints for C_α carbon positions do not necessarily provide sufficient accuracy to form the binding site. Supplementary restraints were required for C_β and imidazole nitrogen distances to produce a valid histidine–zinc binding site. The residues were therefore mutated to the most appropriate His rotamer in the receptor model to ensure that the relative orientations of the residues were correct for coordination with zinc. The restraints used[56] were that C_α carbons should be separated by no more than 11 Å, and the N-N distance should be approximately 6 Å. To allow

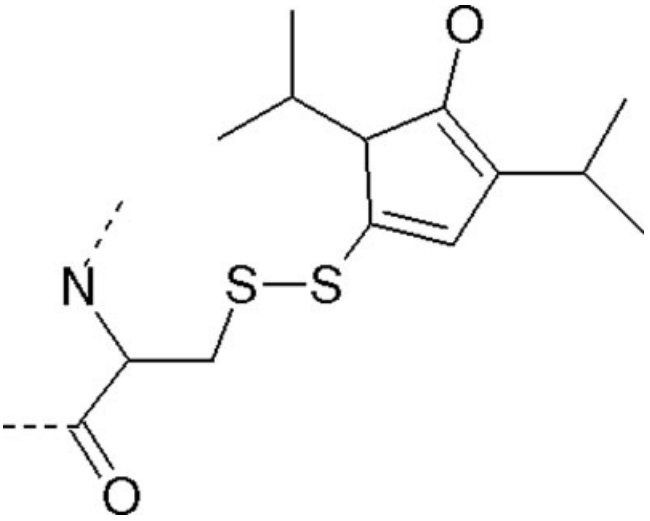

Fig. 1. Chemical structure of the Cys-nitroxide constructed to determine r(C_α-C_α) and r(C_β-C_β) restraints from simulations containing r(O-O) restraints between pairs of nitroxide groups.

proper inclusion of the SDSL data, a nitroxide-substuted cysteine residue was constructed (Fig. 1) so that the relevant r(O-O) distance restraint from Tables I and III could be included explicitly in 100 ps simulations of receptors, each containing a nitroxide pair. In one of the β_2-AR receptors containing a nitroxide at position gn601, the Arg^{131}(gn330)-Glu^{268}(gn600) interaction was broken and the restraint was more readily satisfied than in the other simulations. Consequently, the 100 ps nitroxide simulations were repeated, with the salt bridge broken by an E268A mutation. From these simulations, appropriate r(C_α-C_α) and r(C_β-C_β) restraints were derived, as listed in Tables I and III, and these, rather than the original r(O-O) restraints, are the ones used. The recent ^{19}F NMR study gives complementary information and so was not used here.[57]

Restraint Simulations to Generate Inactive and Active Conformations

The initial receptor model was heated up to 310 K over 50 ps. The initial β_2-AR model was then subjected to restrained MD simulations at 310 K in the presence of either inactive or active restraints (Tables I and III). In the case of the rhodopsin models, only inactive restraints were applied to the cis-retinal bound rhodopsin, and only active restraints were applied to the trans-retinal bound rhodopsin. The restraints were introduced progressively over 100 ps, starting at 1/200 of the restraint energy term and rising progressively every 10 ps. The final 100 ps of MD were conducted in the presence of the restraints at full strength. The structure was then subjected to a conjugate gradient minimization to generate the final inactive or active receptor model. The stability of these final active and inactive structures were assessed (satisfactorily) by performing 100 ps unrestrained MD simulations at 310 K.

Control simulations were run for 1 ns, but these structures did not sample any significantly new conformations [as judged by the root-mean-square (RMS) values]. A simulated annealing protocol was also used in which the structures were heated to 500 K. The restraints were introduced progressively as above, with the final 100 ps of MD conducted in the presence of full-strength restraints. Structures were collected at 10 ps intervals over the subsequent 100 ps. Each of the 10 structures was then cooled to 310 K over 100 ps. After cooling, the structures were minimized and averaged to one structure that was again minimized to generate a final inactive or active receptor model. Thus, while there is no guarantee that the short 310 K simulations have sampled all relevant regions of conformational space, the simulated annealing simulations essentially gave no new structures, again indicating that the sampling in the main 310 K simulations was sufficient.

Molecular Graphics and Structure Validation

The mutations, loop addition, rotamer analysis, and structure validation were carried out using the appropriate modules of WHATIF.[58] In addition, the structures were also validated using the ERRAT program (http://www.doe-mbi.ucla.edu/Services/SV/), which compares the atom positions in the given structure with identical atoms types in a database derived from X-ray structures, and gives a final residue confidence score. ERRAT highlighted a small number of residues in the models as irregular—but fewer than in the rhodopsin crystal structure. It is common to see residues in X-ray crystal structures highlighted as irregular using this type of analysis. In all other respects, including visual checking to ensure that all potential hydrogen-bonding groups were satisfied,[34] the structures satisfied the conditions expected from real protein structures (results not shown).

Simulations, Restraints, and Parameter Derivation

The MD simulations were carried out using the Amber all-atom force field as implemented in AMBER5 and AMBER 7[59] using a nonbonded cutoff of 12 Å and timestep of 0.0005 ps, as in earlier work [37,60,61]; elsewhere, we have found that this earlier force field can yield better results than the force fields designed for full explicit solvation if full explicit solvation is not used. The biochemically derived distance restraints were invoked as either harmonic or half-harmonic restraints, depending on their origin (see Tables I and III), with a force constant of 30 kcal/mol^{-1} $Å^{-2}$. Half-harmonic distance restraints between backbone carbonyl (n) and amide nitrogen (n + 4) of 2.7–3.5 Å were applied to ensure that the α-helical TM structures were maintained; this allows the helix to sample both α-helical and 3_{10}-helical conformations. The electrostatic potential derived charges required for retinol and the nitroxide-modified cysteine spin labels was determined using an in-house version of *rattler*,[62] since this gives charges compatible with AMBER[63]; the additional parameters required were determined by analogy with similar parameters in the AMBER force field.

Docking Methodology

In order to assess the quality of the agonist and antagonist binding sites, we have challenged the models with a set of 172 GPCR ligands using the LigandFit software[64] to determine whether the active model does indeed show a good preference for agonists, while the inactive model retains a preference for antagonists. The ligand set included 14 β-adrenergic agonists, 50 β-adrenergic antagonists, 23 other adrenergic ligands, and 80 nonpeptide ligands comprised of opioid, muscarinic, neurokinin, neurotensin, bradykinin, and serotonin ligands. Being GPCR ligands, these ligands automatically have "drug-like" properties, so the only filtering on the ligand selection was to ensure that the adrenergic and nonadrenergic ligands had a similar molecular mass distribution. The ligand-binding site was defined using the LigandFit flood-filling algorithm,[64] with care taken to ensure that the binding site encompassed the area believed to be occupied by all common ligands (as understood from the site-directed mutagenesis data[37]) and that it was sufficiently large to allow the software to select plausible alternative docking modes. The binding site was primed for docking by interactively docking norepinephrine or S-propranolol (the biologically active enantiomer) into the active or inactive models, respectively, minimizing, running MD simulations for 100 ps, and then carrying out a final minimization. The binding site was also used unprimed and primed with R-propranolol. Given that current virtual screening methods use a rigid enzyme, this step was desirable to ensure that key functional groups, such as the serine OH groups on helix 5, and so forth, were oriented to make productive interactions. The docking used softened nonbonded potentials and, again, this concession was used to make allowances for the standard protocol of using a rigid enzyme, but in other respects the CFF 1.02 force field used by LigandFit is not too dissimilar to that used for the simulations, except that ligand flexibility was implemented by selecting 50,000 random trial conformations, ligand polar hydrogens could rotate in increments of 10°, and the distance-dependent dielectric constant was set to 1/(4r) rather than 1/r. The final ligand conformation was fully minimized within the rigid enzyme. The top 10 conformers were saved subject to a restriction that preserves a degree of diversity in the save list. The average CPU time to process each ligand was 20 min on a Silicon Graphics 400 MHz R1200. The docked poses were ranked using both the docking score (dockscore; based on van der Waals, electrostatic, and ligand internal energy) and the ligscore potentials[64] (LigandFit contains two ligscore potentials, ligscore 1 and ligscore 2; both are based on van der Waals and surface area terms).

RESULTS

Inactive Receptor Conformations

Comparison with the X-ray structure

The RMS difference between the energy-minimized inactive (cis-retinal bound) rhodopsin model and the crystal structure was 3.2 Å (2.2 Å over the TM region), demonstrating that the structure generated with the restrained MD was close to the crystal structure. Predictably, the greatest differences were observed in the intracellular loops (which are less well-defined in the X-ray structure), primarily intracellular loop 2 (IL2), IL3, and the final 5 residues of helix 8. Nevertheless, the loop structure was stable, and the β-sheet formed by residues Arg^{175}-Thr^{177} and Cys^{184}-Ala^{186} (β_2-AR numbers) remained throughout both the rhodopsin and β_2-AR simulations.

The inactive β_2-AR receptor model exhibited slightly larger differences from the crystal structure than did the rhodopsin model, with an RMS difference between the backbone atoms of 3.7 Å (2.6 Å over the TM region). The most notable change was in TM7, with the elimination of a stretch of 3_{10} helix around residue gn723 (gn refers to the GPCRDB[41] generic numbering scheme defined at www.gpcr.org and in Table II, where the first number refers to the helix). This region of the receptor converted into a regular α-helical structure, with a concomitant anticlockwise rotation (as viewed from the extracellular side of the membrane) of the intracellular part of the helix. The most likely reason for requiring a 3_{10} helix in rhodopsin is the stereochemical restraint[65] imposed by the Schiff's base formation between cis-retinal and Lys^{296}. This work commenced before the more recent 1HXZ[66] and 1IL9[67] structures became available, but subsequent comparisons of the three structures show that there is little to gain from repeating all the simulations using these alternative starting structures.

The lack of explicit lipid did not cause the helical bundle to become more compact than the template rhodopsin structure, probably because the interior of the helix bundle and the intraceullular and extracellular loops were solvated. The interhelical distances and tilt angles were comparable to those observed in the rhodopsin crystal structure (results not shown) and other comparable membrane proteins.[68] The amphipathic helix (Asp^{331}-Leu^{342}, denoted helix 8, β_2-AR numbers) was stable throughout the simulations.

Inclusion of nitroxide- and histidine zinc-binding restraints

The distance between the nitroxide radicals placed at the positions listed in Table I in the initial β_2-AR/nitroxide model are similar to those reported in the SDSL studies (Table I). Analysis of the MD trajectories has shown that the nitroxide-reacted cysteine at position Ile^{135}(gn344) is much restricted by the proximity of the intracellular regions of TM5 and TM6; similar observations were made for the 5 corresponding positions in TM6 (gn601–605). This observation (based on simulations in which only one nitroxide pair was introduced so as to reduce the artefacts of the Cys-nitroxide mutant on the natural protein structure and to mimic the SDSL studies) enabled the spin-labeling data to be introduced as C_β-C_β restraints. The time-averaged nature of the SDSL constraints reduces slightly their utility in defining restraints for use in MD simulations compared to the SDCL studies, where a structurally well-defined disulphide bond is formed. However, the results demonstrate that the rhodopsin crystal

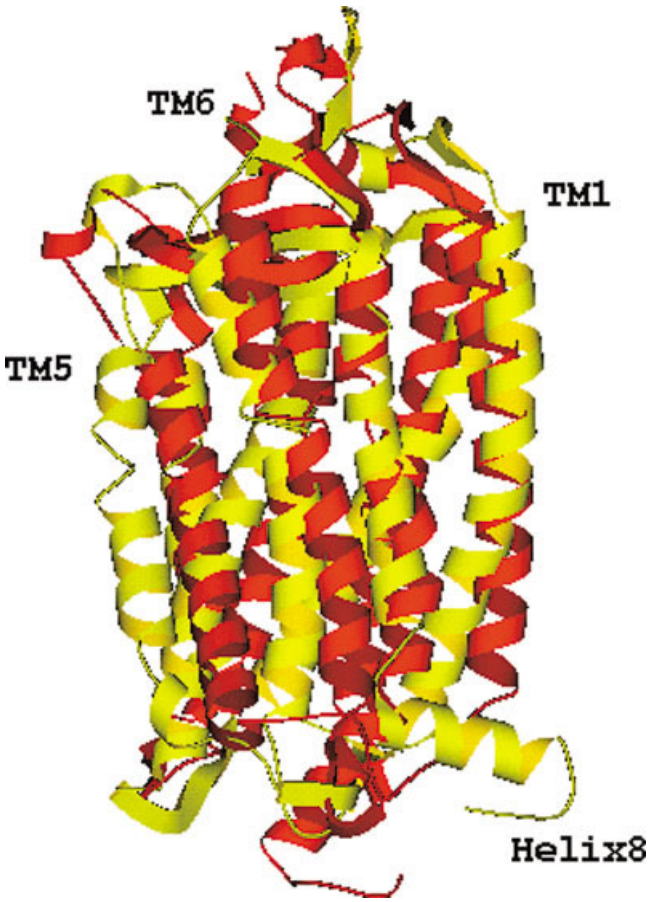

Fig. 2. The inactive rhodopsin model (yellow) superimposed on the active rhodopsin model (red).

structure is consistent with the positions of the Cys-nitroxides, since all the distances observed in the model are similar to those obtained experimentally. The engineered histidine–zinc binding studies in most cases also agreed well with the crystal structure. As with the restraints derived from the SDSL studies, there is some potential ambiguity associated with these restraints because His and Cys can coordinate zinc through bridging water molecules and, as such, the restraint lacks absolute definition.

Active Receptor Conformations

Overall changes

The backbone RMS difference between the final energy-minimized active (trans-retinal bound) rhodopsin model and the crystal structure was 6.2 Å (4.1 Å over the TM helices); the backbone RMS difference between the final energy-minimized active β_2-AR receptor model and the rhodopsin crystal structure and the inactive β_2-AR model was 7.4 Å and 6.2 Å, respectively (the corresponding figures over the transmembrane helices are 4.0 and 3.4 Å respectively). The most notable changes on activation were in TM4, TM5, TM6, TM7, and particularly in helix 8, as shown in Figures 2 and 3; the overall changes are shown schematically in Figure 4. However, detailed analysis of the structural changes on activation (i.e., the nature of helix translation and rotation was not straightforward, as the direction of translation or rotation depends on how the structures were superimposed). (All rotations are described as viewed from the extracellular side of the receptor about an axis roughly perpendicular to the membrane.) Thus, if all the C_α atoms of the TM helical regions of the active and inactive receptor were superimposed, then essentially no rotation was observed for TM5. However, if only TM5 and TM6 were superimposed, then there was anticlockwise rotation of TM5 and clockwise rotation of TM6. Alternative superpositions can reverse the apparent rotation (e.g., on TM6). The origin of these apparent anomalies lies partly in the differential rotation for the intracellular end of TM7 and the extracellular end of TM4, partly in the differential proline positions in rhodopsin and β_2-AR, and partly from the resultant secondary differences in structure. This ambiguity arises also because the true movement is a complex mixture, primarily of translation, but also of bending (especially at proline residues), twisting (e.g., either side of a proline residue), and to a lesser extent rotation. Consequently, while TM6 and TM7 show notable changes on activation, the rotation between TM6 and TM7 is much less than that between TM5 and TM6. These superposition-dependent observations may lead to apparent contradictions between different structural studies that in other respects are in accord with each other.

Nevertheless, several generalizations can be made. TM4 shows a large clockwise rotation in the rhodopsin model because of the crosslink from retinal to Ala^{169} in active state of rhodopsin.[29] Since there are no corresponding photoaffinity labeling data for the β_2-AR, this restraint was only applied to rhodopsin. Nevertheless, the other restraint data result in a diminished but still significant clockwise rotation of TM4. Elsewhere, Nikiforovish and Marshall have shown that the barrier for the rotation of TM4 is low.[69] TM4 also moves slightly away from the bundle, but this is probably because there is less restraint data available for TM4 than for other helices.

TM5 shows little evidence of rotation, except with respect to TM6; inactive TM5 is essentially straight but bends on activation at the highly conserved β_2-AR Pro^{211}(gn520) (97% in the amine family). Initially, a kink around β_2-AR Pro^{288}(gn620), which is part of the CWXP motif and 99% conserved in the amine family, allows either end of TM6 to interact with opposite faces of TM3. On activation, the intracellular end of TM6 moves away from TM2 and TM3 as the Arg(gn340)-Glu(gn600) salt-bridge is broken and in the process, TM6 straightens out, as seen elsewhere.[70] (Mutation of Pro in TM6 causes constitutive activation in the α factor receptor[71].) The straightening of TM6 allows TM5 to move closer, and to some extent the bending in TM5 in the active state mirrors that in TM6. The consequential reduction in the Cys^{265} (TM6)-Lys^{224} (TM5) distance on activation, which Ghanouni et al.[72] related to an increase in fluorescence quenching in β_2-AR, can therefore be interpreted primarily as a change in the tilt angle of helix 6 rather than as a *clockwise* rotation. Similarly, Cys^{265} is accessible in the active but not the inactive structure, and so the SCAM results on a

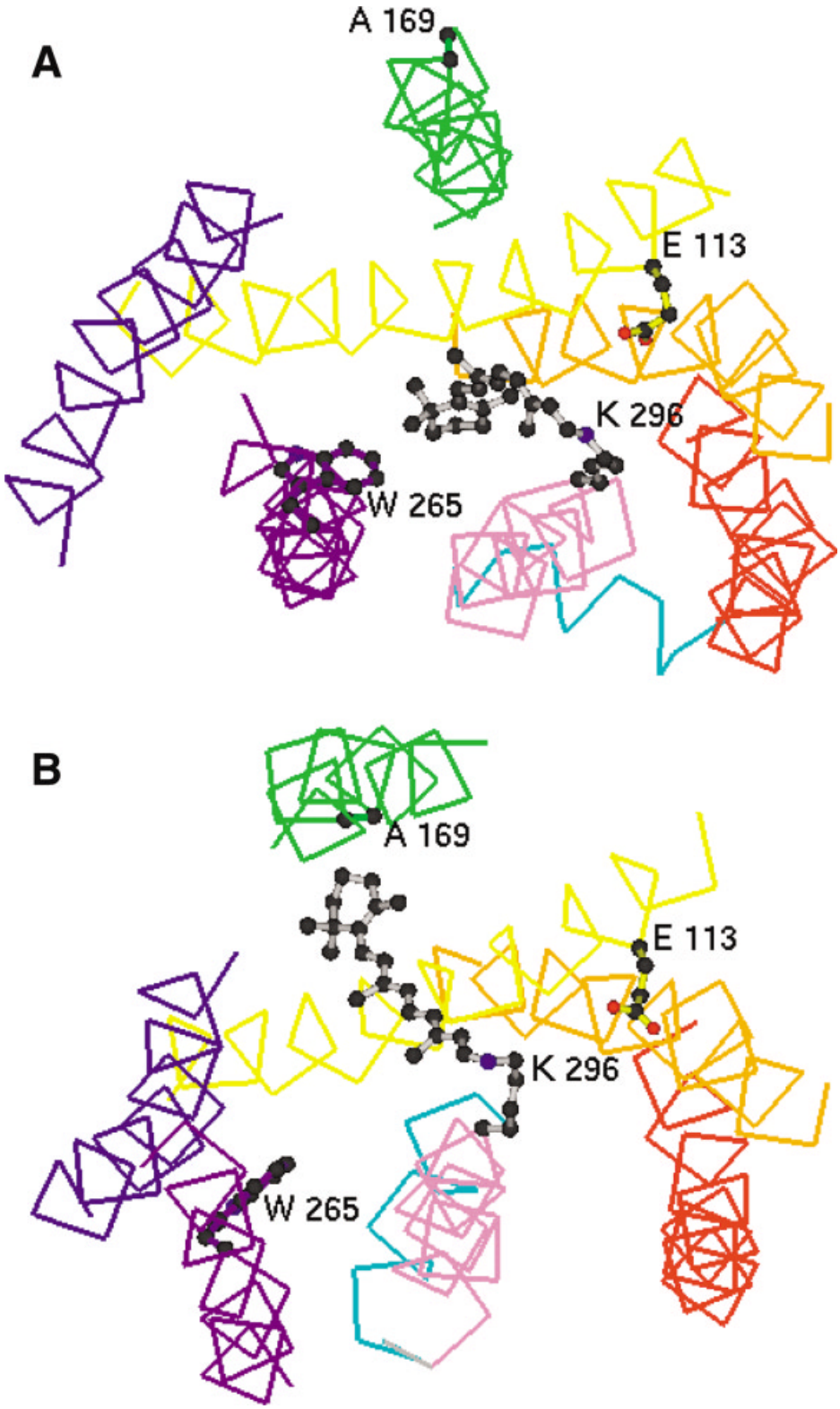

Fig. 3. Position of retinal in the (**A**) inactive and (**B**) active receptor models. Residues identified in the retinal–rhodopsin crosslinking experiments are shown.

constitutively active β_2-AR mutant can also be explained by a change in the tilt angle rather than an *anticlockwise* rotation of TM6.[24] The consequential increase in solvent exposure on activation between the intracellular parts of helices 3 and 6 has been noted elsewhere.[73–76] The rotation, translation, and bending of TM6 permits key residues

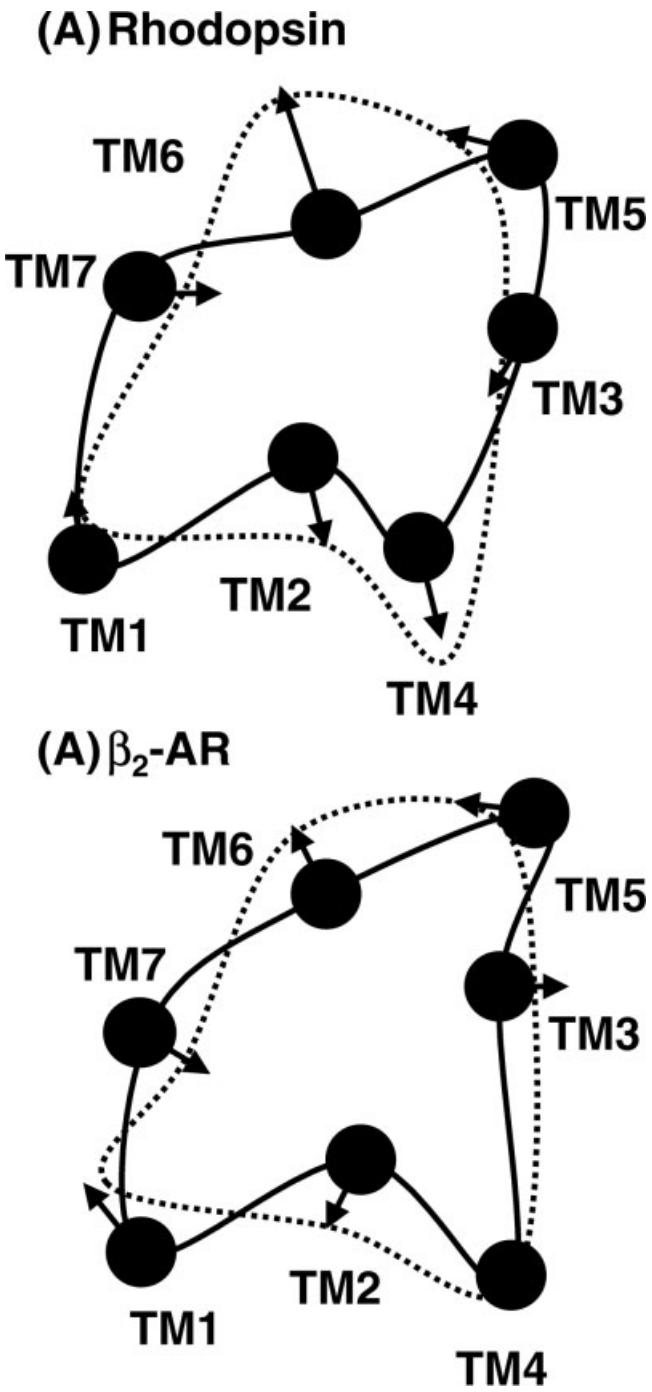

Fig. 4. A schematic representation of the intracellular structural changes occurring on activation for (**A**) rhodopsin and (**B**) the β_2-adrenergic receptor. The intraceullular extent of the inactive structure is shown by a solid black line that joins the intracellular ends of the helices; the corresponding extent of the active structure is shown by a black dotted line. The positions of the helices in the inactive structure are shown as black circles, and the movement is indicated by arrows.

to have differential accessibility toward agonists and antagonists in the active and inactive state, respectively, as discussed below.

Helix 7 is essentially straight in the inactive state,[37] the most recent cryoelectron microscopy structure,[77,78] and the X-ray structure,[1] but the simulations show that it kinks on activation as the intracellular end moves toward TM3 (as TM6 moves away) to help form the Cys^{140}-Cys^{316} rhodopsin disulphide restraint. The flexibility of this region is perhaps due to the Asn^{322}-Pro^{323}(gn730) motif that lies in the vicinity of the kink originally described by Fu et al.[20,35] Indeed, artificially introducing this kink into the starting structure enables the MD simulations to satisfy the active restraints in relatively short simulations, and so it may be that this kink is more relevant to the active structure. This movement of TM7 is the only movement that reduces the exposed intracellular surface area. However, since the Cys^{140}-Cys^{316} rhodopsin disulphide bond is formed under artificial conditions (i.e., on addition of oxidizing agent), it seems that while this crosslink can form, it does not necessarily form in vivo. The consequent large movement seen in helix 8, driven by the restraint between Cys^{140}(gn345) and Cys^{316}(gn743) aided by the kink in TM7, may therefore be interpreted as an increase in mobility of this region.

TM2 shows comparatively less movement, but the intracellular end still moves out on activation from a very central position under the helical bundle close to the intracellular ends of all helices apart from TM5; this movement is aided by a reduction in the bend at Pro^{88}(gn233), so that the intracellular end moves away from TM6. [Pro^{88} is 85% conserved in the biogenic amine receptors but not in the opsins, some of which have a weakly conserved (~30%) GG motif at a similar position (gn230, 231).]

Interactions of Trp^{286} (gn618)

The conserved Trp^{286} (gn618, 97% conserved in the amines) on TM6 plays a key role as it interacts with TM3 and TM7 in the inactive model but moves away from TM7 to interact with TM5 in the active model. (It also interacts with the ligand in many systems.) A glycine in TM7, Gly^{315}(gn722, 75% conserved in amines), provides an ideal space for the indole ring of Trp^{286}(gn618) to occupy, thus reducing steric clashes. Interestingly, position gn722 is 100% conserved as Gly in the adrenergic and dopamine receptors, 100% by Ala in the tachykinin receptors, 97% by Ala in rhodopsin, but 100% by Phe in the neurotensin receptors. Mutation of this Phe to Ala in the human neurotensin NT2 receptor reduces the constitutive activity associated with this subtype (P. Angeloz-Nicoud, personal communication). This implies that a small amino acid (Ala, Gly, Ser, Cys) is required at this position to correctly place Trp(gn618) in the inactive state of the receptor. Gly^{121} and Phe^{261} form a similar pair in the opsins, as shown by compensating mutations in which increases in size at the glycine are compensated by a decrease in size at the phenylalanine.[79,80]

Docking Results

The overall docking results for the most highly ranked conformations are shown in Figure 5. In order to compare these results to other high-quality docking studies, of which Bissantz et al.[81] is a good recent example, we have

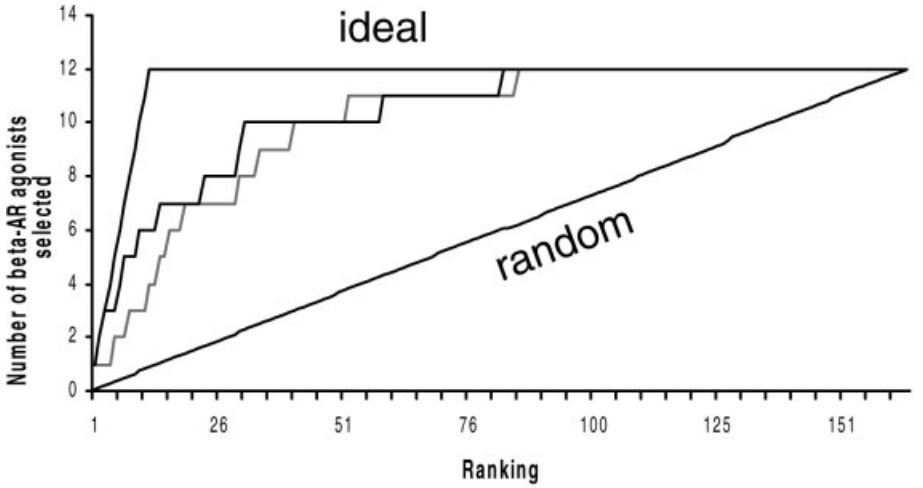

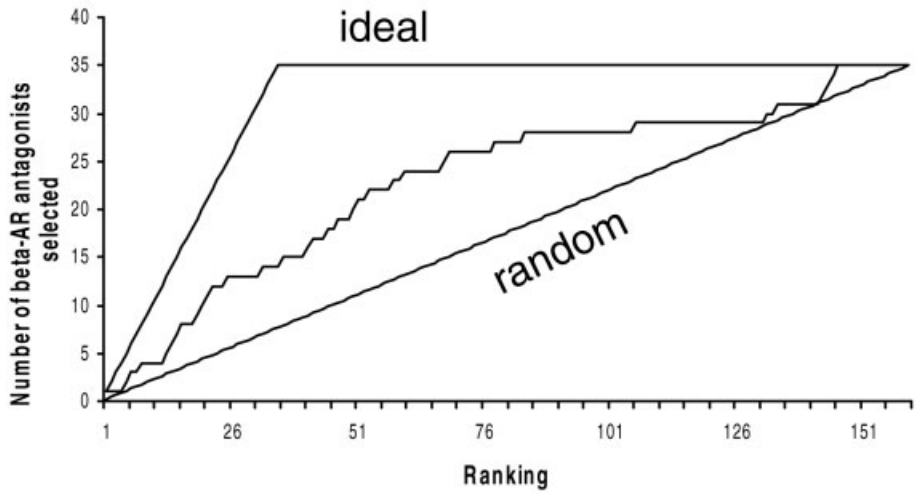

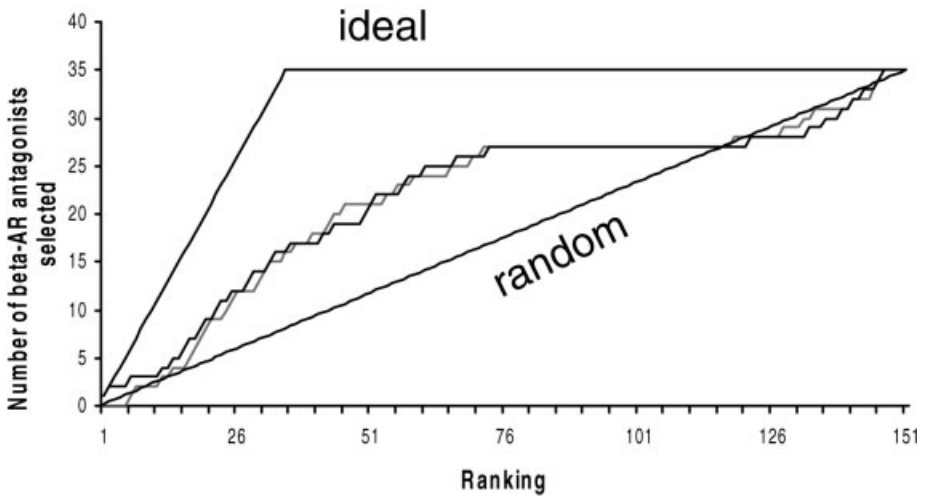

Fig. 5. Enrichment curves for adrenergic ligands docked into (**A**) the norepinephrine-based active structure, (**B**) the s-propranolol-based inactive structure, and (**C**) the inactive apoprotein-based structure. The enrichment curves for the hybrid method are also shown for (A) and (C) in gray. The ideal line, which would result from perfect docking and scoring, and the random line, which would result if the docking results were random, are labeled.

generated 5 hit lists taken from the top 5–25% most highly ranked ligands and determined the hit rate (the proportion of true hits in the hit list) and the yield (the proportion of true hits in the hit list compared to the full ligand list) with a view toward determining the suitability of these structures, particularly the active one, for virtual screening, bearing in mind that while good results do not necessarily by themselves validate the model, they do contribute toward this end. The results are tabulated in Table IV, along with the maximum possible yields, hit rates, and enrichment factors that are attainable with the given number of ligands.

The antagonist results in Figure 5(A and B) show that there is little enrichment until about rank 10; the false positives in this region are primarily opioid ligands. Given the known interactions between adrenergic and opioid receptors,[82,83] it is possible that these are true hits, especially as both receptors share an Asp at position gn322, but we are treating the highly ranked opioid ligands as false positives. Such observations of very highly ranked false positives are quite common in docking studies.

For the agonist results in Figure 5(C), there is immediate enrichment, and the results are very good compared to related studies.[81] Careful examination of the docking mode of the adrenergic agonists and antagonists shows that the results are generally in accord with the known binding mode as determined by site-directed mutagenesis and discussed elsewhere.[37,81] We observed that while ligscore gave very poor enrichment factors (with ligscore 2 giving only marginal improvement over ligscore 1 in these systems), ligscore 1 was superior to dockscore at selecting the correct docking mode from a set of alternative docked conformations. Consequently, we have also ranked the structures according to the dosckscore for the best ligscore conformation. The hit rates, yields, and enrichment factors from this hybrid approach are only slightly inferior to the pure dockscore results but are based on superior structures for some compounds.

While slightly better docking results were obtained when the inactive models were minimized in the presence of an appropriate ligand (norepinephrine or propranolol), the results on the apoprotein-based models provided additional evidence that the lack of explicit lipid did not cause the helical bundle to become more compact than the template rhodopsin structure. It is encouraging that slightly higher enrichment factors were obtained when the inactive model was minimized in the presence of S-propranolol (the biologically active form), whereas slightly lower enrichment factors were obtained when the inactive model was minimized in the presence of R-propranolol.

TABLE IV. Observed Hit Rates, Yields, and Enrichment Factors for Adrenergic Agonists and Antagonists, Along with the Maximum Possible Values That Would Be Obtained With Perfect Structures and Software

	Yield (%)		Hit rate (%)		Enrichment factor	
Hit list (%)	Obs	Max	Obs	Max	Obs	Max
Agonist: active model						
5	42	58	71	100	9.8	13.7
10	58	100	47	100	6.4	10.9
15	67	100	35	100	4.8	7.1
20	83	100	32	100	4.4	5.3
25	83	100	26	100	3.5	4.2
Ave	67	92	42	100	5.8	8.2
Antagonist: S-propranolol-based model						
5	11	23	50	100	2.1	4.3
10	23	46	50	100	2.1	4.3
15	34	69	50	100	2.1	4.3
20	40	91	44	100	1.8	4.3
25	43	100	38	100	1.6	4.1
Ave	30	65	46	100	1.9	4.3
Antagonist apoprotein-based model						
5	9	23	38	100	1.6	4.3
10	17	44	38	100	1.6	4.3
15	31	66	48	100	2.1	4.3
20	40	89	45	100	1.9	4.3
25	49	100	48	100	1.9	3.9
Ave	29	64	43	100	1.8	4.2
Antagonist: R-propranolol-based model						
5	8	23	44	100	1.7	4.3
10	17	46	44	100	1.6	4.3
15	19	69	36	100	1.4	4.3
20	36	91	43	100	1.7	4.3
25	41	100	44	100	1.7	4.1
Ave	23	65	42	100	1.7	4.3
Agonist: active model (hybrid)						
5	17	64	29	100	3.9	13.7
10	42	100	33	100	4.6	10.9
15	58	100	30	100	4.2	7.1
20	67	100	26	100	3.5	5.3
25	75	100	23	100	3.2	4.2
Ave	51	92	28	100	3.9	8.2
Antagonist: apo-based model (hybrid)						
5	6	23	25	100	1.1	4.3
10	11	44	25	100	1.1	4.3
15	26	66	39	100	1.7	4.3
20	40	89	45	100	1.9	4.3
25	49	100	49	100	1.9	3.9
Ave	26	64	36	100	1.5	4.2

The enrichment factor is the number of ligands determined divided by the number expected for a random process (indicated by the dashed line in Fig. 5).

Restraint Redundancy

Thirty-five restraints from a number of different laboratories were used to simulate both the inactive and active receptors. It is interesting to investigate the completeness of the restraints currently available, and so to this end, 10 simulations on the β_2-AR receptor were run with 85% of the active restraints (i.e., 2 chosen at random to be left out) and with the charge on E247 mutated to zero to remove the Arg(gn340)-Glu(gn600) restraining interaction. Several observations are relevant. First, movements of up to 5 Å in the position of helix ends may be observed. Second, differences are observed in helices not directly involved in the

restraints. Third, differences may not necessarily be observed in the helices that are directly involved in the restraints. For example, omission of the Val139Cys-Arg252Cys Cβ (gn344–gn605) and Asp113Cys-Asn312His (gn322–gn719) restraints results in an inward movement of TM2 but surprisingly little movement of TM3. Likewise, omission of the Cys140-Cys316 (gn345–gn743) and Val139Cys-Arg252Cys Cβ (gn344–gn605) restraints affects the contribution of most helices to the opening out of the intracellular part of the helical bundle, but there is very little change to the contribution of TM7. These observations show that the amount and variety of experimental data are not yet sufficient to generate a redundant set of restraints and that additional data, particularly for TM1 and TM4, where the restraints are sparse, would be very useful for generating more accurate models. The importance of each restraint is underlined by the average RMS between the control and the 10 active structures, which is 3.9 ± 0.6 Å (or 3.2 ± 0.6 Å over the transmembrane regions); this compares to an RMS of 6.2 Å between the inactive and active structures. The value of 3.2 ± 0.6 Å is similar to the RMS value of 4.3 Å between the active rhodopsin and active β_2-AR structures, which differ by two restraints, as the β_2-AR does not have the retinol photoaffinity data-derived restraints, while the rhodopsin model does not have the adrenergic ligand-derived restraints. It is also similar to the difference between the inactive structures and the crystal structure.

DISCUSSION

Palmitoylation in the Inactive and Active Receptor Models

In the active receptor models, the Cys^{140}(gn345)-Cys^{316}(gn743) rhodopsin disulfide restraint drives Cys^{341} on helix 8 (the prime palmitoylation site[84]) to lie in close proximity to the intracellular extremities of TMs 3, 5, and 6, as shown in Figure 2. It is unlikely that this interaction is formed continuously in the wild-type active structure in vivo as $Cu(phenantholine)_3^+$ was required as oxidant to form the disulphide bond.[85] The value of this restraint, therefore, is primarily that it shows the increased accessibility of the intracellular end of TM7 to the intracellular end of TM3 following loss of the Arg(gn340)-Glu(gn600) restraining interaction. Functional interpretations beyond inferring increased accessibility are difficult: although Oprian and coworkers did check that some disulphide-linked split rhodopsin receptors activated transducin,[85] this was not checked for the gn345-gn316 disulfide-linked receptor.[26]

One possible inference is that the active model structure shown in Figure 2 may not be consistent with the covalent attachment of palmitate, particularly for receptors palmitoylated at positions N-terminal of Cys^{341}. Figure 2 would therefore appear to contradict the observation that exposure of GPCRs to agonists generally increases the rate of palmitoylation, and this usually results in an increase in palmitoylation levels.[84] Another possible inference is that if helix 8 lies below the helical bundle, this may have negative structural consequences for G-protein coupling, as it would partially block access to the exposed region between TM3 and TM6 observed here and by others who have related this opening to G-protein coupling.[73–76] Such a blocked conformation could underlie the reduced G-protein coupling observed in some depalmitoylated receptors,[84] but the reduced G-protein coupling is more likely to be caused by the phosphorylation of depalmitoylated receptors.[84]

Preferential Interactions With Agonists and Antagonists

The idea that a single template can be representative of all active models (or of all inactive models) is the underlying assumption in this work. Here, with reference to our structures, we examine the evidence for this underlying assumption in the common effects of site-directed mutagenesis at selected key residue positions across a range of receptors that are generally observed to have preferential interactions with agonists and antagonists.

Residue positions gn621 and gn622 are important, as mutation of either can affect ligand binding and signaling.[86,87] Site-directed mutagenesis data indicate that in many receptor families, residue position gn621 is associated with agonist binding and signal transduction[71,88–99] (in that these effects are generally reduced or abolished in mutant receptors), while antagonist binding is not affected by gn621 mutation.[100] In contrast, position gn622 is generally associated with antagonist binding,[101–104] and mutation generally does not affect agonist binding.[103,105–109] In some comprehensive studies, mutation of gn621 only affects agonists, while mutation of gn622 only affects antagonists.[110,111] In some cases, the effect of mutation at gn622 on agonist binding is less than that at gn621[98]). Taken together, the common patterns in the above mutation data on residues gn621 and gn622 support the idea of a generic template, but there are some exceptions recorded below. However, it is often difficult to compare studies, because different agonists and antagonists have different effects, and also because some inverse agonists, which may prefer to bind to the active state, have been described as antagonists.

In a small number of studies, both residues have been mutated, and contrary effects have been observed (e.g., mutation of gn622 affects agonist binding[106,112–114] or does not affect antagonist binding,[115] and mutation of gn621 affects antagonist binding but not agonist binding[116]). While it has also been observed that mutation of gn621 can affect antagonist binding,[117] these are usually nonpeptide antagonists of peptide receptors.[117,118] SCAM studies are equivocal—one indicates that both gn621 and gn622 are accessible to the binding pocket,[119] while another indicates that only gn621 is accessible[88]; the increased exposure of gn621 in our model is in agreement with this overall picture.

Similarly, residue gn718 is associated with agonist binding,[37,120–123] while residue gn719 is associated with antagonist binding.[37,96,124–132] Again, the situation is not clear cut, partly because only a few comprehensive studies have been made, and partly because mutation of gn719 can

lead to misfolded[127] or poorly expressed receptors.[104] These loci have been implicated as conformational switching regions in several receptors, partly because certain amino acid mutations at position gn719 transform antagonists into agonists[96,129] or lead to constitutive activation.[107,133] Nevertheless, the magnitude of the observed changes in this region of the receptor are less than those observed at the intracellular end of helices 6 and 7.

Exceptions to the general mutagenesis pattern include indications that both residues are involved in antagonist binding,[87] or that mutation at gn719 affects agonist binding[114,134–137] or agonist and antagonist binding (but does not necessarily stop signaling),[32,138–142] or binds an inverse agonist in a constitutively active receptor,[143] or does not affect antagonist binding.[115,135,144]

Our model structures are partially in agreement with these observations in that while gn621 and gn719 are exposed in both active and inactive structures, gn622 becomes much less exposed in the active structures, while gn718 becomes more exposed in the rhodopsin active structure, partly as a result of rotational and translational movement, but also through proline bending in TM6. The relationship between these observations and our structural models is partially obscured by the differing helical structure and flexibility of helix 7 in the two models. This inherent flexibility of TM7 may be the origin of the less than clear site-directed mutagenesis effects at these important loci, as indicated by site-directed mutagenesis effects on ligand binding also being observed at position gn720.[126,145] Residue gn722, which is directly below gn719, is also primarily associated with agonist rather than antagonist binding,[146,147] though there are exceptions where there is either little effect [90,105,145] or a preferential effect on antagonists.[116] Again, the increased exposure of gn722 on activation, like that of gn721, is linked to the movement of gn621 that also helps to reduce the exposure of gn622 (and Trp gn618). Likewise, Cys(gn617) is not exposed to the binding cavity in the inactive receptor but becomes exposed on activation, partly as a result of the movement of gn621 and Trp(gn618); this residue has been shown by SCAM methodology to be exposed in a constitutively active mutant,[24] but not in the ordinary receptor.[119]

The Requirement for Multiple GPCR Models

Pharmacological studies show that agonists, antagonists, and inverse agonists do not bind to a single receptor conformation, an observation eloquently elaborated in Gether's recent review[148] of the two state (R/R*) model of GPCR activation.[149] In contrast, earlier models of GPCRs, typically those constructed from cryoelectron microscopy data,[150] failed to distinguish rigorously between an inactive and an active conformation.[33,34] In many cases, one model was used for docking all classes of ligand: agonist, antagonist, and inverse agonist. A comparison of the available models reveals significant differences, usually in the relative helix rotations, helix length, and the depth of key residues within the (implicit) membrane. Some of these differences can be attributed to the fact that data from biophysical studies and site-directed mutagenesis studies on agonist, antagonist, and inverse agonist binding and activity are incorporated into a *single* model. In contrast, pharmacological, biophysical, and structural data, and data on constitutively active receptors,[151] all demonstrate that GPCRs exist in distinguishable conformations and, hence, a single model for any receptor can never be adequate. The usual method to generate an active model is to simulate the conformation changes induced in the presence of an agonist or in the presence of mutations that generate constitutive activity. However, because of limitations in phase space sampling, it is unlikely that the resultant changes from such approaches would be transmitted throughout the structure. Because we have used restraints from most regions of the receptor to generate an active conformation, the problems arising from phase space sampling are likely to be less of a problem with this approach.

Constraining Interactions

Various groups have suggested that the inactive conformation of a receptor is maintained through a network of constraining interactions,[152–154] and that disruption of one of these key constraining interactions might result in a degree of activity being observed.[154] This hypothesis is reinforced by the observation that mutations that cause constitutive activity for a unique receptor signaling pathway can be observed in receptors that naturally couple to multiple distinct signaling pathways.[155] Our simulations support the idea of constraining interactions, and here, the salt bridge between Arg(gn340) and Glu(gn600) presented itself as the main constraining interaction. [Both of these residues are present in the 1F88 crystal structure in a sparsely populated rotameric form but can only interact directly in the refined structure[66] by rotation about torsion χ_1 of the rhodopsin Glu^{247}(gn600) side-chain.] In certain "active" simulations, this salt bridge did not break, and the final structure did not readily satisfy the active restraints. On the other hand, simulations in which this interaction was broken by an E268A (β_2-AR) mutation went a long way toward satisfying the active restraints even if they were not applied (results not shown). Likewise, Arg(gn330)-Glu(gn600) was the only restraining interaction that had to be artificially broken in order to satisfy the active restraints. Constraining interactions, if not dealt with adequately (e.g., through active constraints applied throughout the structure), present a reason why an active receptor model may retain inactive character.

A related observation is the fact that TM6 is alone in having only a single hydrogen bond to other helices,[66] ensuring that there are few constraining interactions. This supports the dynamic role of TM6 in the activation mechanism.

Docking

Generally the docking results presented in Table IV compare very favorably with those of Bissantz et al.,[81] who showed positive evidence that GPCR models can be used in virtual screening. Bissantz et al. generally obtained hit rates of 5–39% and yields (0–70%), particularly for ago-

nists. The following results are particularly relevant. Here, we have used a single docking method rather than an elegantly combined consensus approach. In addition, our ligand list is comprised entirely of GPCR ligands, and has some ligands that are very similar to the β-adrenergic ligands, including α-adrenergic and opioid ligands, which both bind to a highly conserved aspartate on helix 3: These factors would tend to bias our results toward lower enrichment, whereas the Bissantz list contained a significantly more diverse set of compounds. The LigandFit approach used here has been shown to yield results competitive to other methods,[64] but we have no evidence to suggest it is vastly superior to other methods, and so the very favorable results produced here can be partially attributed to the method used to generate the active and inactive structures. It is particularly satisfying that our active structure generating such good results as this represents further divergence away from its rhodopsin parent structure than for the inactive structure. The lower enrichment for the inactive structure is partly a consequence of our observation that the agonists tend to bind to both the active and inactive structure, while the antagonists tend not to bind to the active structure (and this is not merely related to size). It is also possible that antagonists bind to other distinct regions of the receptor (e.g., it appears that the α_{1a}-adrenergic selective antagonists WB 4101 and phentolamine contact residues Q196, I197, and N198 in extracellular loop 2 of the α-adrenergic receptor.[2] Since the receptor was not primed for docking by minimizing a prototype antagonist in that region, this too may contribute to a lower enrichment factor. We anticipate that alternative binding sites are less likely to affect the enrichment factors for agonists. The lower enrichment factors for antagonists compared to agonists (see Fig. 5 and Table IV) may also derive from the labeling of some inverse agonists as antagonists. These docking control studies therefore produce good evidence to support both the structures produced and the method used to generate them. The use of the templates derived from this approach in modeling other GPCRs will be discussed elsewhere.

CONCLUSIONS

Sets of experimental distance restraints were obtained from published site-directed crosslinking, engineered zinc binding, site-directed spin-labeling, IR spectroscopy, and photoaffinity labeling experiments, and rigorously separated into restraints relevant to inactive receptors and those relevant to active receptors. Preliminary simulations showed that the nitroxide labeled substituted cysteine side-chains had limited mobility, permitting incorporation of this data as C_β-C_β restraints.

MD simulations in the presence of either "active" restraints or "inactive" restraints were used to generate two distinguishable receptor models. The active model was satisfactorily generated only after giving due care to releasing the restraining interaction between Arg(gn330)-Glu(gn600). The main changes in the receptor conformation on activation involve TM4, TM5, TM6, and TM7. It is esoterically disappointing that rhodopsin does not show exactly the same changes on activation as the β_2-AR receptor (see Fig. 4), but the main origins of this lie in the different helical content on TM7 and the photoaffinity labeling-derived restraints on TM4 used only for rhodopsin. Nevertheless, the main changes are similar and included significant clockwise rotation of TM4; the displacement of TM6 away from TM3, accomplished by a straightening of TM6, so that it interacts more closely with TM5; increased flexibility in the intracellular half of TM7; and a general opening of the intracellular part of the structure. The differences in structure on activation have been related to selected key loci, namely, positions gn621/gn622 and gn718/gn719 that play different roles in the active and inactive structures.

The β_2-AR active model, in particular, gave high yields, hit rates, and enrichment factors for selecting agonists from related GPCR drug-like ligands in a virtual screen using the LigandFit docking software. These docking results help to validate both the models and the process used to derive them. Our overall conclusions from the docking experiments are in line with those of Bissantz et al.,[81] namely, that homology models of GPCRs offer potential in the rational design of ligands. However, there are still regions such as TM4, where the determination of additional active restraints could significantly improve the modeling process.

In the past, many discrepancies have arisen between models and between models and experiment as a result of failing to identify clearly whether supporting experimental data apply to the active or inactive state; a good example of this is the proposed kink[20,35,37] at the NPXXY motif in TM7, which we propose here applies only to the active state.

SUPPORTING INFORMATION

Receptor coordinates, sequence alignment, analysis of the effect of omitting restraints, Ramachandran plots, and hydrogen-bond analysis of relevant rhodopsin, β_2-AR receptor structures and adrenergic ligands (with CDS (Chemical Data Service, http://cds.dl.ac.uk/cds/cds.html) codes).

REFERENCES

1. Palczewski K, Kumaska T, Hori T, Behnke CA, Motoshima H, Fox BA, Le TI, Teller DC, Okada T, Stenkamp RE, Yamamoto M, Miyano M. Crystal structure of rhodopsin: a G protein-coupled receptor. Science 2000;289:739–745.
2. Zhao MM, Hwa J, Perez DM. Identification of critical extracellular loop residues involved in alpha 1-adrenergic receptor subtype-selective antagonist binding. Mol Pharmacol 1996;50:1118–1126.
3. Altenbach C, Yang K, Farrens DL, Farahbakhsh ZT, Khorana HG, Hubbell WL. Structural features and light-dependent changes in the cytoplasmic interhelical E-F loop region of rhodopsin: a site-directed spin-labeling study. Biochemistry 1996;35:12470–12478.
4. Altenbach C, Cai K, Khorana HG, Hubbell WL. Structural features and light-dependent changes in the sequence 306–322 extending from helix VII to the palmitoylation sites in rhodopsin: a site-directed spin-labeling study. Biochemistry 1999;38:7931–7937.
5. Altenbach C, Klein-Seetharaman J, Hwa J, Khorana HB, Hubbell WL. Structural features and light-dependent changes in the sequence 59–75 connecting helices I and II in rhodopsin: a sitee-directed spin-labeling study. Biochemistry 1999;38:7945–7949.

6. Cai K, Klein-Seetharaman J, Farrens D, Zhang C, Altenback C, Hubbell WL, Khorana HG. Single-cysteine substitution mutants at amino acid positions 306–321 in rhodopsin, the sequence between the cytoplasmic end of helix VII and the palmitoylation sites: sulfhydryl reactivity and transducin activation reveal a tertiary structure. Biochemistry 1999;38:7925–7930.
7. Farahbakhsh ZT, Ridge KD, Khorana HB, Hubbell WL. Mapping light-dependent structural changes in the cytoplasmic loop connecting helices C and D in rhodopsin: a site-directed spin labeling study. Biochemistry 1995;34:8812–8819.
8. Farrens DL, Altenbach C, Yang K, Hubbell WL, Khorana HG. Requirement of rigid-body motion of transmembrane helices for light activation of rhodopsin. Science 1996;274:768–770.
9. Klein-Seetharaman J, Hwa J, Cai K, Altenbach C, Hubbell WL, Khorana HG. Single- cysteine substitution mutants at amino acid positions 55–75, the sequence connecting the cytoplasmic ends of helices I and II in rhodopsin: reactivity of the sulfhydryl groups and their derivatives identifies a tertiary structure that changes upon light-activation. Biochemistry 1999;38:7938–7944.
10. Langen R, Cai K, Altenback C, Khorana HB, Hubbell WL. Structural features of the C-terminal domain of bovine rhodopsin: a site-directed spin-labeling study. Biochemistry 1999;38: 7918–7924.
11. Yang K, Farrens DL, Altenbach C, Farahbakhsh ZT, Hubbell WL, Khorana HB. Structure and function in rhodopsin—cysteines 65 and 316 are in proximity in a rhodopsin mutant as indicated by disulfide formation and interactions between attached spin labels. Biochemistry 1996;35:14040–14046.
12. Yang K, Farrens DL, Hubbell WL, Khorana HG. Structure and function in rhodopsin: single cysteine substitution mutants in the cytoplasmic interhelical E-F loop region show position-specific effects in transducin activation. Biochemistry 1996;35: 12464–12469.
13. Elling CE, Schwartz TW. Connectivity and orientation of the seven helical bundle in the tachykinin NK-1 receptor probed by zinc site engineering. EMBO J 1996;15:6213–6219.
14. Elling CE, Thirstrup K, Nielsen SM, Hjorth SA, Schwartz TW. Engineering of metal-ion sites as distance constraints in structural and functional analysis of 7TM receptors. Fold Des 1997;2: S76–S80.
15. Lu ZL, Hulme EC. A network of conserved intramolecular contacts defines the off-state of the transmembrane switch mechanism in a seven-transmembrane receptor. J Biol Chem 2000;275:5682–5686.
16. Sheikh SP, Vilardarga JP, Baranski TJ, Lichtarge O, Iiri T, Meng EC, Nissenson RA, Bourne HR. Similar structures and shared switch mechanisms of the beta2-adrenoceptor and the parathyroid hormone receptor: Zn(II) bridges between helices III and VI block activation. J Biol Chem 1999;274:17033–17041.
17. Elling CE, Thirstrup K, Holst B, Schwartz TW. Conversion of agonist site to metal-ion chelator site in the beta(2)-adrenergic receptor. Proc Natl Acad Sci USA 1999;96:12322–12327.
18. Rosenkilde MM, Lucibello M, Holst B, Schwartz TW. Natural agonist enhancing bis-His zinc-site in transmembrane segment V of the tachykinin NK3 receptor. FEBS Lett 1998;439:35–40.
19. Thirstrup K, Elling CE, Hjorth SA, Schwartz TW. Construction of a high affinity zinc switch in the kappa-opioid receptor. J Biol Chem 1996;271:7875–7878.
20. Fu D, Ballesteros JA, Weinstein H, Chen J, Javitch JA. Residues in the seventh membrane-spanning segment of the dopamine D2 receptor accessible in the binding-site crevice. Biochemistry 1996;35:11278–11285.
21. Javitch JA, Li X, Kaback J, Karlin A. A cysteine residue in the third membrane-spanning segment of the human D_2 receptor is exposed in the binding-site crevice. Proc Natl Acad Sci USA 1994;91:10355–10359.
22. Javitch JA, Fu DY, Chen JY. Residues in the fifth membrane-spanning segment of the dopamine D2 receptor exposed in the binding-site crevice. Biochemistry 1995;34:16433–16439.
23. Simpson MM, Ballesteros JA, Chiappa V, Chen JY, Suehiro M, Hartman DS, Godel T, Snyder LA, Salmar TP, Javitch JA. Dopamine D4/D2 receptor selectivity is determined by a divergent aromatic microdomain contained within the second, third, and seventh membrane-spanning segments. Mol Pharmacol 1999; 56:1116–1126.
24. Javitch JA, Fu DY, Liapakis G, Chen JY. Constitutive activation of the beta(2) adrenergic receptor alters the orientation of its sixth membrane-spanning segment. J Biol Chem 1997;272: 18546–18549.
25. Kono M, Yu H, Oprian DD. Disulfide bond exchange in rhodopsin. Biochemistry 1998;37:1302–1305.
26. Yu H, Kono M, Oprian DD. State-dependent disulfide cross-linking in rhodopsin. Biochemistry 1999;38:12028–12032.
27. Zeng FY, Hopp A, Soldner A, Wess J. Use of a disulfide cross-linking strategy to study muscarinic receptor structure and mechanisms of activation. J Biol Chem 1999;274:16629–16640.
28. Struthers M, Yu H, Kono M, Oprian DD. Tertiary interactions between the fifth and sixth transmembrane segments of rhodopsin. Biochemistry 1999;38:6597–6603.
29. Borhan B, Souto ML, Imai H, Shichida Y, Nakanishi K. Movement of retinal along the visual transduction path. Science 2000;288:2209–2212.
30. Darrow JO, Hadac EM, Miller LJ, Sugg EE. Structurally similar small molecule photoaffinity CCK-A agonists and antagonists as novel tools for directly probing 7TM receptor–ligand interactions. Bioorg Med Chem Lett 1998;8:3127–3132.
31. Dong MQ, Dings XQ, Pinon DI, Hadac EM, Oda RP, Landers JP, Miller LJ. Structurally related peptide agonist, partial agonist, and antagonist occupy a similar binding pocket within the cholecystokinin receptor—rapid analysis using fluorescent photoaffinity labeling probes and capillary electrophoresis. J Biol Chem 1999;274:4778–4785.
32. Ji ZS, Hadac EM, Henne RM, Patel SA, Lybrand TP, Miller LJ. Direct identification of a distinct site of interaction between the carboxyl-terminal residue of cholecystokinin and the type A cholecystokinin receptor using photoaffinity labeling. J Biol Chem 1997;272:24393–24401.
33. Scheer A, Cotecchia S. Constitutively active G protein-coupled receptors: potential mechanisms of receptor activation. J Recept Signal Transduct Res 1997;17:57–73.
34. Pogozheva ID, Lomize AL, Mosberg HI. The transmembrane 7-alpha-bundle of rhodopsin: distance geometry calculations with hydrogen bonding constraints. Biophys J 1997;72:57–73.
35. Konvicka K, Guarnieri F, Ballesteros JA, Weinstein H. A proposed structure for transmembrane segment 7 of G protein-coupled receptors incorporating an Asn-Pro/Asp-Pro motif. Biophys J 1998;75:601–611.
36. Zhou W, Flanagan C, Ballesteros JA, Konvicka K, Davidson JS, Weinstein H, Miller RP, Sealfon SC. A reciprocal mutation supports helix 2 and helix 7 proximity in the gonadotropin-releasing hormone receptor. Mol Pharmacol 1994;45:165–170.
37. Gouldson PR, Snell CR, Reynolds CA. A new approach to docking in the beta 2-adrenergic receptor that exploits the domain structure of G-protein-coupled receptors. J Med Chem 1997;40: 3871–3886.
38. Donnelly D, Findlay JB, Blundell TL. The evolution and structure of aminergic G protein-coupled receptors. Receptors Channels 1994;2:61–78.
39. Donnelly D, Maudsley S, Gent JP, Moser RN, Hurrell CR, Findlay JB. Conserved polar residues in the transmembrane domain of the human tachykinin NK2 receptor: functional roles and structural implications. Biochem J 1999;339:55–61.
40. Palczewski K, Kumasake T, Hori T, Behnke CA , Motoshima H, Fox BA, Trong I, Teller DC, Okada T, Stenkamp RE, Yamamoto M, Miyano M. Crystal structure of rhodopsin: a G-protein-coupled receptor. Nature 2000;289:739–745.
41. Horn F, Weare J, Beukers MW, Horsch S, Bairoch A, Chen W, Edvardsen O, Campagne F, Vriend G. GPCRDB: an information system for G protein-coupled receptors. Nucleic Acids Res 1998; 26:275–279.
42. Oliveira L, Paiva AM, Vriend G. A common motif in G-protein-coupled seven transmembrane helix receptors. J Comput Aided Mol Des 1993;7:649–658.
43. Harris M, Kihlen M, Bywater RP. PLIM: a protein–ligand interaction modeller. J Mol Recogn 1993;6:111–115.
44. Iadanza M, Holtje M, Ronsisvalle G, Holtje HD. Kappa-opioid receptor model in a phospholipid bilayer: molecular dynamics simulation. J Med Chem 2002;45:4838–4846.
45. Tang P, Xu Y. Large-scale molecular dynamics simulations of general anesthetic effects on the ion channel in the fully hydrated membrane: the implication of molecular mechanisms of general anesthesia. Proc Natl Acad Sci USA 2002;99:16035–16040.
46. Tajkhorshid E, Nollert P, Jensen MO, Miercke LJW, O'Connell J, Stroud RM, Schulten K. Control of the selectivity of the aqua-

porin water channel family by global orientational tuning. Science 2002;296:525–530.
47. Im W, Roux B. Ions and counterions to a biological channel: a molecular dynamics simulation of OmpF porin from *Escherichia coli* in an explicit membrane with 1 M KCl aqueous salt solution. J Mol Biol 2002;319:1177–1197.
48. Capener CE, Sansom MSP. Molecular dynamics simulations of a K channel model: sensitivity to changes in ions, waters, and membrane environment. J Phys Chem B 2002;106:4543–4551.
49. Rohrig UF, Guidoni L, Rothlisberger U. Early steps of the intramolecular signal transduction in rhodopsin explored by molecular dynamics simulations. Biochemistry 2002;41:10799–10809.
50. Kong YF, Ma JP. Dynamic mechanisms of the membrane water channel aquaporin-1 (AQP1). Proc Natl Acad Sci USA 2001;98: 14345–14349.
51. Dehner A, Planker E, Gemmecker G, Broxterman Q B, Bisson W, Formaggio F, Crisma M, Toniolo C, Kessler H. Solution structure, dimerization, and dynamics of a lipophilic alpha/3(10)-helical, C-alpha-methylated peptide: implications for folding of membrane proteins. J Am Chem Soc 2001;123:6678–6686.
52. Goetz M, Carlotti C, Bontems F, Dufourc EJ. Evidence for an alpha-helix → pi-bulge helicity modulation for the neu/erB-2 membrane-spanning segment: a H-1 NMR and circular dichroism study. Biochemistry 2001;40:6534–6540.
53. Johnson ET, Parson WW. Electrostatic interactions in an integral membrane protein. Biochemistry 2002;41:6483–6494.
54. Lin JH, Baker NA, McCammon JA. Bridging implicit and explicit solvent approaches for membrane electrostatics. Biophys J 2002; 83:1374–1379.
55. Higaki JN, Fletterick RJ, Craik CS. Engineered metalloregulation in enzymes. Trends Biochem Sci 1992;17:100–104.
56. Gouldson PR, Snell CR, Reynolds CA. A new approach to docking in the β_2-adrenergic receptor that exploits the domain structure of G-protein-coupled receptors. J Med Chem 1997;40:3871–3886.
57. Loewen MC, Klein-Seetharaman J, Getmanova EV, Reeves PI, Schwalbe H, Khorana HG. Solution 19F nuclear Overhauser effects in structural studies of the cytoplasmic domain of mammalian rhodopsin. Proc Natl Acad Sci USA 2001;98:4888–4892.
58. Vriend G. WHATIF: a molecular modelling and drug design program. J Mol Graph 1990;8:52–56.
59. Weiner SJ, Kollman PA, Case DA, Singh UC, Ghio C, Algona G, Profeta S, Weiner P. A new force field for molecular mechanical simulations of nucleic acids and proteins. J Am Chem Soc 1984;106:765–784.
60. Gouldson PR, Reynolds CA. Simulations on dimeric peptides—evidence for domain swapping in G-protein-coupled receptors. Biochem Soc Trans 1997;25:1066–1071.
61. Gouldson PR, Snell CR, Bywater RP, Higgs C, Reynolds CA. Domain swapping in G-protein coupled receptor dimers. Protein Eng 1998;11:1181–1193.
62. Ferenczy GG, Reynolds CA, Richards WG. Semiempirical AM1 electrostatic potentials and AM1 electrostatic potential derived charges—a comparison with ab initio values. J Comput Chem 1990;11:159–169.
63. Reynolds CA, Ferenczy GG, Richards WG. Methods for determining the reliability of semiempirical electrostatic potentials and potential derived charges. J Mol Struct (THEOCHEM) 1992;88: 249–269.
64. Venkatachalam CM, Jiang X, Oldfield T, Walkman M. LigandFit: a novel method for the shape-directed rapid docking of ligands to protein active sites. J Mol Graph Model 2003;21:289–307.
65. Pappin DJ, Findlay JBC. Sequence variability in the retinal-attachment domain of mammalian rhodopsins. Biochem J 1984; 217:605–613.
66. Teller DC, Okada T, Behnke CA, Palczewski K, Stenkamp RE. Advances in determination of a high-resolution three-dimensional structure of rhodopsin, a model of G-protein-coupled receptors (GPCRs). Biochemistry 2001;40:7761–7772.
67. Okada T, Fujiyoshi Y, Silow M, Navarro J, Landau EM, Shichida Y. Functional role of internal water molecules in rhodopsin revealed by X-ray crystallography. Proc Natl Acad Sci USA 2002;99:5982–5987.
68. Bywater RP, Thomas D, Vriend G. A sequence and structural study of transmembrane helices. J Comput Aided Mol Des 2001;15:533–552.
69. Nikiforovish GM, Marshall GR. Three-dimensional model for meta-II rhodopsin, an activated G-protein coupled receptor. Biochemistry 2003;42:9110–9120.
70. Singh R, Hurst DP, Barnett-Norris J, Lynch DI, Reggio H. Activation of the cannabinoid CB1 receptor may involve a W6.48/F3.36 rotamer toggle switch. J Pept Res 2002;60:357–370.
71. Dube P, DeCostanzo A, Konopka JB. Interaction between transmembrane domains five and six of the alpha-factor receptor. J Biol Chem 2000;275:26492–26499.
72. Ghanouni P, Steenhuis JJ, Farrens DL, Kobilka BK. Agonist-induced conformational changes in the G-protein-coupling domain of the beta 2 adrenergic receptor. Proc Natl Acad Sci USA 2001;98:5997–6002.
73. Yeagle PL, Albert AD. A conformational trigger for activation of a G protein by a G-protein-coupled receptor. Biochemistry 2003;42: 1365–1368.
74. Choi G, Landin J, Galan JF, Birge RR, Albert AD, Yeagle PL. Structural studies of metarhodopsin II, the activated form of the G-protein coupled receptor, rhodopsin. Biochemistry 2002;41: 7318–7324.
75. Angelova K, Fanelli F, Puett D. A model for constitutive lutropin receptor activation based on molecular simulation and engineered mutations in transmembrane helices 6 and 7. J Biol Chem 2002;277:32202–32213.
76. Greasley PJ, Fanelli F, Scheer A, Abuin L, Nenniger-Tosato M, DeBenedetti PG, Cotecchia S. Mutational and computational analysis of the alpha(1b)-adrenergic receptor: involvement of basic and hydrophobic residues in receptor activation and G protein coupling. J Biol Chem 2001;276:46485–46494.
77. Baldwin JM, Schertler GF, Unger VM. An alpha-carbon template for the transmembrane helices in the rhodopsin family of G-protein-coupled receptors. J Mol Biol 1997;272:144–164.
78. Unger VM, Hargrave PA, Baldwin JM, Schertler GF. Arrangement of rhodopsin transmembrane alpha-helices. Nature 1997; 389:203–206.
79. Han M, Lin SW, Minkova M, Smith SO, Sakmar TP. Functional interaction of transmembrane helices 3 and 6 in rhodopsin—replacement of phenylalanine 261 by alanine causes reversion of phenotype of a glycine 121 replacement mutant. J Biol Chem 1996;271:32337–32342.
80. Han M, Lou JH, Nakanishi K, Sakmar TP, Smith SO. Partial agonist activity of 11-cis-retinal in rhodopsin mutants. J Biol Chem 1997;272:23081–23085.
81. Bissantz C, Bernard P, Hibert M, Rognan D. Protein-based virtual screening of chemical databases: II. Are homology models of G-protein coupled receptors suitable targets? Proteins 2003;50: 5–25.
82. Jordan BA, Trapaidze N, Gomes I, Nivarthi R, Devi LA. Oligomerization of opioid receptors with beta 2-adrenergic receptors: a role in trafficking and mitogen-activated protein kinase activation. Proc Natl Acad Sci USA 2002;98:343–348.
83. McVey M, Ramsay D, Kellett E, Rees S, Wilson S, Pope AJ, Milligan G. Monitoring receptor oligomerization using time-resolved fluorescence resonance energy transfer and bioluminescence resonance energy transfer: the human delta-opioid receptor displays constitutive oligomerization at the cell surface, which is not regulated by receptor occupancy. J Biol Chem 2001;276:14092–14099.
84. Qanbar R, Bouvier M. Role of palmitoylation/depalmitoylation reactions in G-protein-coupled receptor function. Pharmacol Therapeut 20033333;97:1–33.
85. Yu HB, Oprian DD. Tertiary interactions between transmembrane segments 3 and 5 near the cytoplasmic side of rhodopsin. Biochemistry 1999;38:12033–12040.
86. Hovelmann S, Hoffmann SH, Kuhne R, ter Laak T, Reilander H, Beckers T. Impact of aromatic residues within transmembrane helix 6 of the human gonadotropin-releasing hormone receptor upon agonist and antagonist binding. Biochemistry 2002;41:1129–1136.
87. Cotte N, Balestre MN, Aumelas A, Mahe E, Phalipou S, Morin D, Hibert M, Manning M, Durroux T, Barberis C, Mouillac B. Conserved aromatic residues in the transmembrane region VI of the V-1A vasopressin receptor differentiate agonist vs. antagonist ligand binding. Eur J Biochem 2000;267:4253–4263.
88. Chen S, Xu M, Lin F, Lee D, Riek P, Graham RM. Phe 310 in transmembrane VI of the alpha1B-adrenergic receptor is a key

switch residue involved in activation and catecholamine ring aromatic bonding. J Biol Chem 1999;274:16320–16330.
89. Escrieut C, Gigoux V, Archer E, Verrier S, Maigret B, Behrendt R, Moroder L, Bignon E, Silvente-Poirot S, Pradayrol L, Fourmy D. The biologically crucial C terminus of cholecystokinin and the non-peptide agonist SR-146,131 share a common binding site in the human CCK1 receptor—evidence for a crucial role of Met-121 in the activation process. J Biol Chem 2002;277:7546–7555.
90. Blaker M, Ren Y, Seshadri L, McBride EW, Beinborn M, Kopin AS. CCK-B/gastrin receptor transmembrane domain mutations selectively alter synthetic agonist efficacy without affecting the activity of endogenous peptides. Mol Pharmacol 2000;58:399–406.
91. Vogel WK, Sheehan DM, Schimerlik MI. Site-directed mutagenesis on the m2 muscarinic acetylcholine receptor: the significance of Tyrr403 in the binding of agonists and functional coupling. Mol Pharmacol 1997;52:1087–1094.
92. Mosser Va, Amana IJ, Schimerlik MI. Kinetic analysis of M-2 muscarinic receptor activation of G(i) in Sf9 insect cell membranes. J Biol Chem 2002;277:922–931.
93. Wess J, Maggio R, Palmer JR, Vogel Z. Role of conserved threonine and tyrosine residues in acetylcholine binding and muscarinic receptor activation—a study with M3-muscarinic-receptor point mutants. J Biol Chem 1992;267:19313–19319.
94. Karnik SS, Husain A, Graham RM. Molecular determinants of peptide and non-peptide binding to the AT(1) receptor. Clin Exp Pharmacol Physiol 1996;23:S58–S66.
95. Nakayama TA, Khorana HG. Mapping of the amino acids in membrane-embedded helices that interact with the retinal chromophore in bovine rhodopsin. J Biol Chem 1991;266:4269–4275.
96. Meng F, Wei Q, Hoversten MT, Taylor LP, Akil H. Switching agonist/antagonist properties of opiate alkaloids at the delta opioid receptor using mutations based on the structure of the orphanin FQ receptor. J Biol Chem 2000;275:21939–21945.
97. Lin YM, Jian XY, Lin ZL, Krooggg GS, Mantey S, Jensen RT, Battey J, Northrup J. Two amino acids in the sixth transmembrane segment of the mouse gastrin-releasing peptide receptor are important for receptor activation. J Pharmacol Exp Ther 2000;294:1053–1062.
98. Yang YK, Dickinson C, Haskell Luevano C, Gantz I. Molecular basis for the interaction of [Nle(4),D-Phe(7)]melanocyte stimulating hormone with the human melanocortin-1 receptor (melanocyte alpha-MSH receptor). J Biol Chem 1997;272:23000–23010.
99. Chen CH, Chen WY, Liu HL, Liu TT, Tsou AP, Lin CY, Chao T, Qu Y, Hsiao KJ. Identification of mutations in the arginine vasopressin receptor 2 gene causing nephrogenic diabetes insipidus in Chinese patients. J Hum Genet 2002;47:66–73.
100. Berglund MM, Fredriksson R, Salaneck E, Larhammar D. Reciprocal mutations of neuropeptide Y receptor Y2 in human and chicken identify amino acids important for antagonist binding. FEBS Lett 2002;518:5–9.
101. Olah ME, Ren HZ, Ostrowski J, Jacobson KA, Stiles GL. Cloning, expression, and characterization of the unique bovine-A1 adenosine receptor—studies on the ligant-binding site by site-directed mutagenesis. J Biol Chem 1992;267:10764–10770.
102. Mollereau C, Moisand C, Butour JL, Parmentier M, Meunier JC. Replacement of Gln(280) by His in TM6 of the human ORL1 receptor increases affinity but reduces intrinsic activity of opioids. FEBS Lett 1996;395:17–21.
103. Huang XP, Nagy PI, Williams FE, Peseckis SM, Messer WS. Roles of threonine 192 and asparagine 382 in agonist and antagonist interactions with M-1 muscarinic receptors. Br J Pharmacol 1999;126:735–745.
104. Wieland K, Ter Laak AM, Smit MJ, Kuhne R, Timmerman H, Leurs R. Mutational analysis of the antagonist-binding site of the histamine H-1 receptor. J Biol Chem 1999;274:29994–30000.
105. Fernandez LM, Puett D. Identification of amino acid residues in transmembrane helices VI and VII of the lutropin choriogonadotropin receptor involved in signaling. Biochemistry 1996;35:3986–3993.
106. Shin N, Coates E, Murgolo NJ, Morse KL, Bayne M, Strader CD, Monsma FJ. Molecular modeling and site-specific mutagenesis of the histamine-binding site of the histamine H-4 receptor. Mol Pharmacol 2002;62:38–47.
107. Spivak CE, Beglan CL, Seidleck BK, Hirshbein LD, Blaschak CJ, Uhl GR, Surratt CK. Naloxone activation of mu-opioid receptors mutated at a histidine residue lining the opioid binding cavity. Mol Pharmacol 1997;52:983–992.
108. Gao ZG, Chen A, Barak D, Kim SK, Muller CE, Jacobson KA. Identification by site-directed mutagenesis of residues involved in ligand recognition and activation of the human A(3) adenosine receptor. J Biol Chem 2002;277:19056–19063.
109. Feighner SD, Howard AD, Prendergast K, Palyha OC, Hreniuk DL, Nargund R, Underwood D, Tata JR, Dean DC, Tan CP, McKee KK, Woods JW, Patchett AA, Smith RG, Van der Ploeg LHT. Structural requirements for the activation of the human growth hormone secretagogue receptor by peptide and nonpeptide secretagogues. Mol Endocrinol 1998;12:137–145.
110. Nardone J, Hogan PG. Delineation of a region in the B2 bradykinin receptor that is essential for high-affinity agonist binding. Proc Natl Acad Sci USA 1994;91:4417–4421.
111. Ward SDC, Curtis CAM, Hulme EC. Alanine-scanning mutagenesis of transmembrane domain 6 of the M-1 muscarinic acetylcholine receptor suggests that Tyr381 plays key roles in receptor function. Mol Pharmacol 1999;56:1031–1041.
112. Manivet P, Schneider B, Smith JC, Choi DS, Maroteaux L, Kellermann O, Launay JM. The serotonin binding site of human and murine 5-HT2B-receptors—molecular modeling and site-directed mutagenesis. J Biol Chem 2002;277:17170–17178.
113. Berthold M, Kahl U, Jureus A, Kask K, Nordvall G, Langel U, Bartfai T. Mutagenesis and ligand modification studies on galanin binding to its GTP-binding protein-coupled receptor GalR1. Eur J Biochem 1997;249:601–606.
114. Jiang QL, Guo DP, Lee BX, VanRhee AM, Kim YC, Nicholas RA, Schachter JB, Harden TK, Jacobson KA. A mutational analysis of residues essential for ligand recognition at the human P2Y(1) receptor. Mol Pharmacol 1997;52:499–507.
115. Moro S, Guo DP, Camaioni E, Boyer JL, Harden TK, Jacobson KA. Human P2Y(1) receptor: molecular modeling and site-directed mutagenesis as tools to identify agonist and antagonist recognition sites. J Med Chem 1998;41:1456–1466.
116. Labbe-Jullie C, Barroso S, Nicolas-Eteve D, Reversat JL, Botto JM, Mazella J, Bernassau JM, Kitabgi P. Mutagenesis and modeling of the neurotensin receptor NTR1: identification of residues that are critical for binding SR 48692, a nonpeptide neurotensin antagonist. J Biol Chem 1998;273:16351–16357.
117. Greenfeder S, Cheewatrakoolpong B, Billah M, Egan RW, Keene E, Murgolo NJ, Anthes JC. The neurokinin-1 and neurokinin-2 receptor binding sites of MDL103,392 differ. Bioorg Med Chem 1999;7:2867–2876.
118. Giolitti A, Cucchi P, Renzetti AR, Rotondaro L, Zappitelli S, Maggi CA. Molecular determinants of peptide and nonpeptide NK-2 receptor antagonists binding sites of the human tachykinin NK-2 receptor by site-directed mutagenesis. Neuropharmacology 2000;39:1422–1429.
119. Javitch JA, Ballesteros JA, Weinstein H, Chen J. A cluster of aromatic residues in the sixth membrane-spanning segment of the dopamine D2 receptor is accessible in the binding-site crevice. Biochemistry 1998;37:998–1006.
120. Akeson M, Sainz E, Mantey SA , Jensen RT, Battey JF. Identification of four amino acids in the gastrin-releasing peptide receptor that are required for high affinity agonist binding. J Biol Chem 1997;272:17405–17409.
121. Gardella TJ, Luck MD, Fan MH, Lee CW. Transmembrane residues of the parathyroid hormone (PTH)/PTH-related peptide receptor that specifically affect binding and signaling by agonist ligands. J Biol Chem 1996;271:12820–12825.
122. Jensen CJ, Gerard NP, Schwartz TW, Gether U. The species selectivity of chemically distinct tachykinin nonpeptide antagonists is dependent on common divergent residues of the rat and human neurokinin-1 receptors. Mol Pharmacol 1994;45:294–299.
123. Sainz E, Akeson M, Mantey SA, Jensen RT, Battey JF. Four amino acid residues are critical for high affinity binding of neuromedin B to the neuromedin B receptor. J Biol Chem 1998;273:15927–15932.
124. Parker EM, Grisel DA, Iben LG, Shapiro RA. A single amino-acid difference accounts for the pharmacological distinctions between the rat and human 5-hydroxytryptamine 1B receptors. J Neurochem 1993;60:380–383.
125. Glennon RA, Dukat M, Westkaemper RB, Ismaiel AM, Izzarelli DB, Parker EM. The binding of propranolol at 5-hydroxytryptamine(1D beta) T355N mutant receptors may

involve formation of two hydrogen bonds to asparagine. Mol Pharmacol 1995;49:198–206.
126. Stithama J, Stojanovic A, Merenick BL, O'Hara KA, Hwa J. The unique ligand-binding pocket for the human prostacyclin receptor—site-directed mutagenesis and molecular modeling. J Biol Chem 2003;278:4250–4257.
127. Dragic T, Trkola A, Thompson DAD, Cormier EG, Kajumo FA, Maxwell E, Lin SW, Ying WW, Smith SO, Sakmar TP, Moore JP. A binding pocket for a small molecule inhibitor of HIV-1 entry within the transmembrane helices of CCR5. Proc Natl Acad Sci USA 2000;97:5639–5644.
128. Waugh DJJ, Gaivin RJ, Zuscik MJ, Gonzalez-Cabrera P, Ross SA, Yun J, Perez DM. Phe-308 and Phe-312 in transmembrane domain 7 are major sites of alpha(1)-adrenergic receptor antagonist binding—imidazoline agonists bind like antagonists. J Biol Chem 2001;276:25366–25371.
129. Suryanarayana S, Kobilka BK. Amino acid substitutions at position 312 in the seventh hydrophobic segment of the beta 2-adrenergic receptor modify ligand-binding specificity. Mol Pharmacol 1993;44:111–114.
130. Gerber BO, Meng EC, Dotsch V, Baranski TJ, Bourne HR. An activation switch in the ligand binding pocket of the C5a receptor. J Biol Chem 2001;276:3394–3400.
131. Weitz CJ, Nathans J. Rhodopsin activation—effects on the metarhodopsin-I metarhodopsin-II equilibrium of neutralization or introduction of charged amino acids within putative transmembrane segments. Biochemistry 1993;32:14176–14182.
132. Liang XY, Parkinson JA, Weishaupl M, Gould RO, Paisey SJ, Park HS, Hunter TM, Blindauer CA, Parsons S, Sadler PJ. Structure and dynamics of metallomacrocycles: recognition of zinc xylyl-bicyclam by an HIV coreceptor. J Am Chem Soc 2002;124:9105–9112.
133. Rim J, Oprian DD. Constitutive activation of opsin—interaction of mutants with rhodopsin kinase and arrestin. Biochemistry 1995;34:11938–11945.
134. Lundstrom K, Turpin MP, Large C, Robertson G, Thomas P, Lewell XQ. Mapping of dopamine D-3 receptor binding site by pharmacological characterization of mutants expressed in CHO cells with the Semliki Forest virus system. J Recept Signal Transduct Res 1998;18:133–150.
135. Gouldson P, Legoux P, Carillon C, Delpech B, Le Fur G, Ferrara P, Shire D. Contrasting roles of Leu(356) in the human CCK(1) receptor for antagonist SR 27897 and agonist SR 146131 binding. Eur J Pharmacol 1999;383:339–346.
136. Donohue PJ, Sainz E, Akeson M, Kroog GS, Mantey SA, Battey JP, Jensen RT, Northrup JK. An aspartate residue at the extracellular boundary of TMII and an arginine residue in TMVII of the gastrin-releasing peptide receptor interact to facilitate heterotrimeric G protein coupling. Biochemistry 1999; 38:9366–9372.
137. Mirzadegan T, Diehl F, Ebi B, Bhakta S, Polsky I, McCarley D, Mulkins M, Weatherhead GS, Lapierre JM, Dankwardt J, Morgans D, Wilhelm R, Jarnagin K. Identification of the binding site for a novel class of CCR2b chemokine receptor antagonists—binding to a common chemokine receptor motif within the helical bundle. J Biol Chem 2000;275:25562–25571.
138. Lu ZL, Saldanha JW, Hulme EC. Transmembrane domains 4 and 7 of the M-1 muscarinic acetylcholine receptor are critical for ligand binding and the receptor activation switch. J Biol Chem 2001;276:34098–34104.
139. Kopin AS, McBride EW, Quinn SM, Kolakowski LF, Beinborn M. The role of the cholecystokinin-B gastrin receptor transmembrane domains in determining affinity for subtype-selective ligands. J Biol Chem 1995;270:5019–5023.
140. Owens CE, Akil H. Determinants of ligand selectivity at the kappa-receptor based on the structure of the orphanin FQ receptor. J Pharmacol Exp Ther 2002;300:992–999.
141. Meng, Taylor LP, Hoversten MT, Ueda Y, Ardati A, Reinscheid RK, Monsma FJ, Watson SJ, Civelli O, Akil H. Moving from the orphanin FQ to an opioid receptor using four point mutations. J Biol Chem 1996;271:32016–32020.
142. Meng F, Ueda Y, Hoversten MT, Taylor LP, Reinscheid RK, Monsma FJ, Watson SJ, Civelli O, Akil H. Creating a functional opioid alkaloid binding site in the orphanin FQ receptor through site-directed mutagenesis. Mol Pharmacol 1998;53:772–777.
143. Casarosa P, Menge WM, Minisini R, Otto C, van Heteren J, Jongejan A, Timmerman H, Moepps B, Kirchoff F, Mertens T, Smit MJ, Leurs R. Identification of the first nonpeptidergic inverse agonist for a constitutively active viral-encoded G protein-coupled receptor. J Biol Chem 2003;278:5172–5178.
144. Gouldson PR, Legoux P, Carillon C, Delpech B, Le Fur G, Ferrara P, Shire D. Contrasting roles of Leu^{356} in the human CCK_1 receptor for antagonist SR 27897 and agonist SR 146131 binding. Eur J Pharmacol 1999;383:341–348.
145. Kedzie KM, Donello JE, Krauss HA, Regan JW, Gil DW. A single amino-acid substitution in the EP2 prostaglandin receptor confers responsiveness to prostacyclin analogs. Mol Pharmacol 1998;54:584–590.
146. Dalpiaz A. Townsend-Nicholson A, Beukers MW, Schofield PR, Ijzerman AP. Thermodynamics of full agonist, partial agonist, and antagonist binding to wild type and mutant adenosine A(1) receptors. Biochem Pharmacol 1998;56:1437–1445.
147. Kim JH, Wess J, VanRhee AM, Schoneberg T, Jacobson KA. Site-directed mutagenesis identifies residues involved in ligand recognition in the human A(2A) adenosine receptor. J Biol Chem 1995;270:13987–13997.
148. Gether U, Kobilka BK. G protein-coupled receptors: II. Mechanism of agonist activation. J Biol Chem 1998;273:17979–17982.
149. De Lean A, Stadel JM, Lefkowitz RJ. A ternary complex model explains the agonist-specific binding properties of the adenylate cyclase-coupled beta-adrenergic receptor. J Biol Chem 1980;255: 7108–7117.
150. Krebs A, Villa C, Edwards PC, Schertler GFX. Characterisation of an improved two-dimensional p22121 crystal from bovine rhodopsin. J Mol Biol 1998;282:991–1003.
151. Kjelsberg MA, Cotecchia S, Ostrowski J, Caron MG, Lefkowitz RJ. Constitutive activation of the alpha 1B-adrenergic receptor by all amino acid substitutions at a single site: evidence for a region which constrains receptor activation. J Biol Chem 1992; 267:1430–1433.
152. Porter JE, Hwa J, Perez DM. Activation of the alpha1b-adrenergic receptor is initiated by disruption of an interhelical salt bridge constraint. J Biol Chem 1996;271:28318–28323.
153. Kim JM, Altenbach C, Thurmond RL, Khorana HG, Hubbell WL. Structure and function in rhodopsin: rhodopsin mutants with a neutral amino acid at E134 have a partially activated conformation in the dark state. Proc Natl Acad Sci USA 1997;94:14273–14278.
154. Hulme EC, Lu ZL, Ward SD, Allman K, Curtis CA. The conformational switch in 7-transmembrane receptors: the muscarinic receptor paradigm. Eur J Pharmacol 1999;375:247–260.
155. Perez DM, Hwa J, Gaivin R, Mathur M, Borwn F, Graham RM. Constitutive activation of a single effector pathway: evidence for multiple activation states of a G protein-coupled receptor. Mol Pharmacol 1996;49:112–122.
156. Elling CE, Nielsen SM, Schwartz TW. Conversion of antagonist-binding site to metal-ion site in the tachykinin NK-1 receptor. Nature 1995;374:74–77.
157. Beck M, Sakmar TP, Siebert F. Spectroscopic evidence for interaction between transmembrane helices 3 and 5 in rhodopsin. Biochemistry 1998;37:7630–7639.
158. Gouldson PR, Winn PJ, Reynolds CA. A molecular dynamics approach to receptor mapping—application to the $5HT_3$ and β_2-adrenergic receptors. J Med Chem 1995;38:4080–4086.